AD-A243 727

(12)

REPORT D(

Form Approved
OMB No. 0704-0188

1. AGENCY USE ONLY (Leave blank)	2. REPORT DATE	3. REPORT TYPE AND DATES COVERED
	10-31-91	Final Technical 15 Feb 89 - 14 Aug 90

4. TITLE AND SUBTITLE

(U) On the Origin and Control of Large Coherent Structures in Turbulent Shear Flow

5. FUNDING NUMBERS

PE - 61102F
PR - 2307
SA - BS
G - AFOSR - 89 - 0307

6. AUTHOR(S)

A. Seifert and I. Wygnanski

7. PERFORMING ORGANIZATION NAME(S) AND ADDRESS(ES)

Department of Fluid Mechanics and Heat Transfer
Tel Aviv University
Ramat Aviv ISRAEL

8. PERFORMING ORGANIZATION REPORT NUMBER

9. SPONSORING/MONITORING AGENCY NAME(S) AND ADDRESS(ES)

AFOSR/NA
Building 410
Bolling AFB DC 20332-6448

10. SPONSORING/MONITORING AGENCY REPORT NUMBER

AFOSR
89-0307

11. SUPPLEMENTARY NOTES

12a. DISTRIBUTION/AVAILABILITY STATEMENT

Approved for public release; distribution is unlimited

12b. DISTRIBUTION CODE

13. ABSTRACT (Maximum 200 words)

The inhibition of two-dimensional Tollmien-Schlichting waves by active means is well known. Surface deformation, heat input and mechanical means were used to impose disturbances on the boundary layer which have an opposite phase to the waves existing in the flow. Thus, transition might be delayed by suppressing the amplitude of these waves. Natural disturbances in boundary layers start as three dimensional wave-packets, because they originate at surface imperfections or are precipitated by temporal disturbances in the incoming stream. The possibilities of controlling such disturbances are being currently investigated. In this context the spatial interaction among three dimensional wave trains, emanating from discrete point-sources, in a boundary layer are discussed. Only a local wave attenuation is feasible by activating two harmonic, point-source disturbances anywhere in the boundary layer. This was shown theoretically for a variety of locations, separation distances and phase delays between the two sources and proven experimentally when the disturbance sources were displaced along the span. The spanwise phase gradients of the disturbances, linked to the streamwise distance from their point-source present a major obstacle to such a simple attenuation scheme. These difficulties cannot be foreseen by considering 3-D perturbations. Spatially distributed control mechanisms are therefore required for the purpose of delaying the amplification of concentrated three dimensional disturbances.

14. SUBJECT TERMS

Boundary Layer, Stability, Transition

15. NUMBER OF PAGES

36

16. PRICE CODE

17. SECURITY CLASSIFICATION OF REPORT	18. SECURITY CLASSIFICATION OF THIS PAGE	19. SECURITY CLASSIFICATION OF ABSTRACT	20. LIMITATION OF ABSTRACT
Unclassified	Unclassified	Unclassified	UL

NSN 7540-01-280-5500

Standard Form 298 (Rev. 2-89) Prescribed by ANSI Std. Z39-18
298-102

TRANSITION TO TURBULENCE IN A LAMINAR BOUNDARYLAYER AND ITS RELATION TO LARGE COHERENT STRUCTURES IN TURBULENT FLOW.

A Narrative summary

by:

I. Wygnanski

Observations of natural transition is experimentally simple though unproductive method of investigating the phenomenon because of the complexity of the interaction among many processes that occur almost simultaneously during the latter stages of transition. The theoretical analysis leading to the transition process has its origin in idealized two dimensional wave-like perturbations which, at best are modulated along the span. These models, when backed by experiments (e.g. Klebanoff et al. 1962; Kachanov et al. 1977; Saric & Reynolds 1980) predict the evolution of non linearities and they provide the notion that an interaction between streamwise and spanwise travelling waves is one of the prime causes of transition.

A different experimental approach was tried out by Gaster & Grant (1975) on the supposition that transition originates from a momentary disturbance which is highly concentrated in a small space namely at a point. This supposition may stress the non linear aspects of the problem because, even a low-energy disturbance originating by a short impulse at a point, might contain sufficiently high amplitudes of various Fourier components so as to bypass the Tollmien-Schlichting process and interact instantly with the surrounding boundary layer by destabilizing it and contaminating it with turbulence. We think that this is the manner in which turbulent spots originate and spread in a laminar boundary layer.

We have been studying the spot over the past 15 years and related its rate of spread and internal structure to known stability concepts. The relationship between the shape of the spot and its size to the secondary breakdown of the Tollmien-Schlichting wavepacket generated by the spot was proven (Glezer, Katz and Wygnanski 1989). The effect of pressure gradient on the rate of spread of the spot and on the shape of its boundaries was established (Katz, Seifert and Wygnanski 1990) and it turned out that

favorable pressure gradient has a major impact on the breakdown process. We are in a possession of detailed data pertaining to the internal structure of the spot which has still to be properly analized (A. Seifert's M.Sc. thesis was not published). The perseverence of the the turbulent spot in a turbulent boundary layer and its probable connection to the large coherent structures prevailing in the outer region of a turbulent boundary layer was shown in the seventies (Zilberman Wygnanski and Kaplan 1977) but since that time we had been preoccupied with charting the structure of the spot in a laminar environment. Consequently the interaction of the spot with the turbulence surrounding it, was not pursued in recent years in spite of the apparent usefulness of this approach.

It is quite possible that the transition process is accelerated by the interaction of disturbances originating from different point-sources in the boundary layer. In order to assess the severity of these interactions and separate their effect from other interactions resulting from either the three dimensionality of the disturbances or from their finite amplitude the following three part experiment was undertaken. In it only the nature of the interactions resulting from the superposition of two, small amplitude disturbances were considered. These disturbances emanated from separate "point-sources" located at different spanwise coordinates on a flat plate. The spatial interactions between two continuous wave trains as well as between two wave packets were investigated and special attention was paid to the linear aspects of this process. Any deviations from linearity were carefully scrutinized.

A study of the evolution of a disturbance emanating from a single harmonic point-source in a Blasius boundary layer, was initially repeated in order to confirm and expand the available data base and provide a quick comparison for further studies. These measurements were performed at Reynolds numbers varying between $850 < R_{\delta^*} < 1200$. The three-dimensional, harmonic disturbance is amenable to a fairly simple linear analysis provided that the background flow is parallel and the amplitude of the disturbance is small. The eigen functions measured directly downstream of the "point source" are essentially two-dimensional and agree very well with the calculated eigen-functions for this case. The spanwise distribution of the maximum amplitude of the most prominent wave (i.e. a wave whose dimensionless frequency was $F=104*10^{-4}$ at $990<R_{\delta^*}<1200$) has a saddle point directly downstream of the source and two maxima located along the rays of $Z/X=0.08$. The double hump appearance of the spanwise amplitude distribution was shown to depend on the frequency and on the

Reynolds number. The present results are in substantial agreement with the measurements of Kachanov and with the linear calculations of Mack. The shape of the measured amplitudes and phases of the streamwise velocity perturbations changes considerably along the span due to the coupling between the Orr-Sommerfeld modes and vertical vorticity modes. The measurements are in good agreement with the calculated linear, three-dimensional eigen functions. The harmonic point source disturbance evolves in space according to the linear model provided the forcing amplitude does not exceed 3% within the range of R_{δ^*} considered, or less than 1% far downstream from the source.

The interactions of two harmonic wave-trains emanating with the same phase, amplitude and frequency from two sources which are only displaced along the span were investigated in the second stage of the experiment. Surveys of velocity fluctuations were made at various distances from both sources. The data for each survey was recorded three times: once while both harmonic disturbances were simultaneously activated and twice when only one of the disturbances was alternately activated. Only in this manner one could asses the validity of the linear superposition of these perturbations. At sufficiently low amplitudes of the initial harmonic perturbation, a complex summation of the waves emanating from each source separately, represented quite well the flow pattern observed when both sources operated concurrently.

Wave cancellation by two harmonic point-source disturbances originating from different locations on the surface (i.e. displaced in both x and z) are virtually impossible due to the steep spanwise phase gradients of the waves further downstream. This type of difficulty was not encountered whenever the perturbations were two-dimensional. Consequently, much more sophisticated control mechanisms are required in order to delay the amplification of three dimensional disturbances in the direction of streaming than hitherto contemplated.

In the second stage of this experiment, the continuous oscillatory perturbation was replaced by a pulse, which in turn, generated a wave packet emanating from a point source. The excitation amplitudes were low enough so that the streamwise evolution of the disturbance was essentially linear over a considerable distance. The amplitude and phase of each Fourier component of the perturbation in the packet was identical to the corresponding perturbation in the wave train, even the appearance of the double-hump in the spanwise distribution of amplitudes reoccurred in the wave packet for the predominant frequency observed. The flow field associated with the packet was not only mapped outside the boundary layer, as it was done by Gaster, but all

across the boundary layer and in particular near the critical layer (near the surface) where the amplitudes are high.

When the spanwise interaction of two wave packets was considered, a weakly non linear interaction was noticed at large values of R_{δ^*} for the lowest wave numbers considered. The coexistence of a broad spectrum of velocity fluctuations in the interacting wave packets may produce a large number of secondary interactions which are not feasible during the interaction of two harmonic wave trains. It appears that the subharmonic form of interaction emerges as being the leading one in the range of parameters considered.

References

Klebanoff, P.S., Tidstrom, K.D. and Sargent, L.M. (1962) "The Three Dimensional Nature of Boundary Layer Instability" JFM 12, 1.

Kachanov, Y.S. and Levchenko V.Y. (1984) "The resonant Interaction at Laminar Turbulent transition in a Boundary Layer" JFM vol 138, 209

Saric, W.S. and Thomas, A.S.W. (1983) "Experiments on the Subharmonic Rours to Turbulence in Boundary Layer" Proceedings on IUTAM Symposium on Turbulence and Chaotic Phenomena in Fluid Kyoto Japan

Gaster, M. and Grant, I. (1975) "An Experimental Investigation of the Formation and Development of a wave Packet in a Laminar Boundary Layer" Proc. Roy. Soc. A. 347, 253 London

Glezer, A., Katz, Y. and Wygnanski, I. (1989) "On the Breakdown of a Wave Packet Trailing the Turbulent Spot in a Laminar Boundary Layer" JFM 198, 1

Y. Katz, A. Seifert and I. Wygnanski "On the Evolution of a Turbulent Spot in a Laminar Boundary Layer with Favourable Pressure Gradient" J. Fluid Mechanics (1990) vol. 221 pp. 1

Zilberman, M., Wygnanski I.,and Kaplan R.E. (1976) On the Evolution of a Transitional Spot in a Turbulent Boundary layer Phys.Fluid Suppl.

List of Personnel

A. Seifert; B. Nishri; I. Wygnanski

List of Publications

A. Seifert and I. Wygnanski "On the Interaction of Wave Trains Emanating from Two Point Sources in a Blasius Boundary Layer" Proceedings of the Royal Aeronautical Society Symposiium on Transition - Cambridge 1991

Y. Katz, A. Seifert and I. Wygnanski "On the Evolution of a Turbulent Spot in a Laminar Boundary Layer with Favourable Pressure Gradient" J. Fluid Mechanics (1990) vol. 221 pp. 1

A. Glezer, Y. Katz and I. Wygnanski "ON the Breakdown of a Wave Packet Trailing the Turbulent Spot in a Laminar Boundary Layer" J. Fluid Mechanics (1989) vol. 198 pp. 1

APPENDIX A

On The Interaction of Wave Trains Emanating From Two Point Sources In A Blasius Boundary Layer

by A Seifert and I Wygnanski

ON THE INTERACTION OF WAVE TRAINS EMANATING FROM TWO POINT SOURCES IN A BLASIUS BOUNDARY LAYER

A. Seifert and I. Wygnanski
Dep. of Fluid Mech. and Heat Transfer
Faculty of Engineering, Tel-Aviv University
Ramat-Aviv, 69978 ISRAEL
Fax: 972-3-5414540 or 5413752

Abstract

The inhibition of two-dimensional Tollmien-Schlichting waves by active means is well known. Surface deformation, heat input and mechanical means were used to impose disturbances on the boundary layer which have an opposite phase to the waves existing in the flow. Thus, provided that two-dimensional T-S waves lead to turbulence, transition might be delayed by suppressing the amplitude of these waves. Natural disturbances in boundary layers are manifested as three dimensional wave-packets, because they originate at surface imperfections and are precipitated by temporal disturbances in the incoming stream. The possibilities of controlling such disturbances are being currently investigated. In this context the spatial interaction among three dimensional wave trains, emanating from discrete point-sources, in a Blasius boundary layer are discussed.

The evolution of an isolated harmonic disturbance emanating from a point-source was initially considered in order to provide a reference for the more complex configurations. The experiments were done at Reynolds numbers varying between $820 < R_{\delta^*} < 1150$ and the data was compared to linear calculations assuming that the background flow is parallel and the amplitude of the disturbance is small. The measurements validated the linear calculations within the range of amplitudes and R_{δ^*} considered. They are also in substantial agreement with the measurements of Kachanov (Ref. 1) and with the predictions of Mack (Ref. 2).

The investigation of the interaction between two harmonic wave-trains emanating, with the same amplitude and frequency, from two point-sources displaced along the span followed. The validity of the linear superposition of these disturbances was confirmed experimentally because, at sufficiently low amplitudes of the initial harmonic perturbation, a complex summation of the waves emanating from each source separately, also represented the resulting flow pattern when both sources operated concurrently.

Only a local wave attenuation is feasible by activating two harmonic, point-source disturbances anywhere in the boundary layer. This was shown theoretically for a variety of locations, separation distances and phase delays between the two sources and proven experimentally when the disturbance sources were displaced along the span. The spanwise phase gradients of the disturbances, linked to the streamwise distance from their point-source present a major obstacle to such a simple attenuation scheme. These difficulties could not be foreseen by considering two-dimensional perturbations. Spatially distributed control mechanisms are therefore required for the purpose of delaying the amplification of concentrated three dimensional disturbances, either steady or pulsating, with increasing R_{δ^*}.

List of Symbols

A	Amplitude, [% of U_∞]
c	Phase velocity, $c=\omega/\alpha$
f	frequency, [Hz]
F	dimensionless frequency, $F=\frac{2\pi f\nu}{U_\infty^2}\times10^6$
R_{δ^*}	Reynolds number, $R_{\delta^*}=(U_\infty\ \delta^*)/\nu$
Re_x	Reynolds number, $Re_x=(U_\infty\ X)/\nu$
Re_z	Reynolds number, $Re_x=(U_\infty\ Z)/\nu$
U	mean velocity in X direction
u	fluctuating X component of velocity
V,v	Y component of velocity
W,w	Z component of velocity
X	streamwise coordinate
X_s	streamwise distance from disturbance source
X_p	X location of disturbance source
Y	coordinate normal to the wall
Y_{ma}	Y of disturbance maximum amplitude
Z	spanwise coordinate
Z_s	spanwise distance from disturbance source, $Z_s=Z-Z_p$
Z_p	Z location of disturbance source

Greek

α_r	real part of streamwise wavenumber, $\alpha_r=2\pi/\lambda_x$
α_i	amplification factor
β	spanwise wavenumber, real, $\beta=2\pi/\lambda_z$
δ^*	boundary layer displacement thickness
ζ_y	vertical component of vorticity
κ	3D wave number, $\kappa^2=\alpha^2+\beta^2$
λ_x	streamwise wavelength
λ_z	spanwise wavelength
ν	kinematic viscosity
ϕ	phase
Ψ	stream functions
χ	complex phase
ω	circular frequency, $\omega=2\pi f$

Abbreviations

FSP	Falkner-Skan Parameter, usually labeled β, $\beta=2m/(m+1)$, where $U_\infty \propto X^m$
HPS	A harmonic disturbance emanating from an isolated Harmonic-Point-Source
MA	Maximum Amplitude
THPS	A harmonic disturbance emanating from Two-Harmonic-Point-Sources
TS	Tollmein-Schlichting waves
2D	Two Dimensional
3D	Three Dimensional

Introduction

Background

Velocity perturbations occurring naturally in a boundary layer are seldom harmonic or two dimensional. They often originate at surface imperfections and are precipitated by temporally random disturbances in the free stream. Nevertheless, the most detailed information available about the growth or decay of disturbances in boundary layers focuses on a somewhat artificial case of a harmonic motion in two dimensions. The current understanding of the possible means of controlling such disturbances is even more restricted. Tollmien-Schlichting waves of identical frequency, emanating from two, 2D harmonic sources displaced in the direction of streaming, may either reinforce or weaken one another depending on the phase relationship between them. The possibility of wave cancellation is attractive because it may be used to delay the transition from laminar to turbulent flow. Two dimensional wave interactions were first investigated by Wehrmann (Ref. 3), by Liepmann et. al (Ref. 4), Thomas (Ref. 5) and most recently by Popator and Saric (Ref. 6). A single mode of oblique waves could be controlled in a similar manner.

A suppression of complex 3D disturbances originating randomly by a variety of sources represents a difficult task. Isolated disturbances emanating from a single point source were studied by Gaster (Refrences 7 and 8) and Mack (Ref. 2), following some pioneering work of Benjamin (Ref. 9) and of Criminale and Kovasznay (Ref. 10). The disturbances investigated are either continuous or time dependent and consequently they were generated by either a harmonic point-source or by a pulse. Gaster (Ref. 7) showed that three dimensional wave-packets, constituting of a finite band of frequencies and spanwise wave numbers propagating in a boundary layer, can be generated by a localized impulsive disturbance (e.g. a brief and a tiny vertical jet). Such a disturbance produces a flat, broad-band spectrum which is selectively amplified by the boundary layer to contain a dominant band of 2D and 3D wave numbers. Gaster's theoretical model was based on the integration of eigen modes calculated from the Orr-Sommerfeld equation making use of Squire's theorem (Ref. 11). These calculations resembled the observed, initial development of the wave-packet at the outer edge of the boundary layer (Ref. 8).

Mack and Kendall (Ref. 2) and Kachanov (Ref. 1) investigated the evolution of a wave train produced by an harmonic-point-source (HPS) in a Blasius boundary layer. Mack's calculations indicated that the maximum amplitude of the disturbance lies on the ray emanating from the source and defined by $Z_S / X_S = 0.05$ to 0.09 (for F=60 at R_{δ^*}=800 to 1000), rather than on the plane of symmetry as expected from the simplified interpretation of Squire's theorem. These calculations are in good agreement with experimental observations (References 1 and 2).

The interaction between two wave trains emanating from spatially separated, two harmonic-point-sources located in a fully developed Blasius boundary layer is considered presently. It is a much simpler type of interaction than the one occurring between wave packets yet it contains some important three dimensional ingredients which need to be considered in any attempt of active control of the transition process. This simpler kind of interaction enables us to study separately the effect of three dimensionality, finite amplitude and wide frequency content which are all present simultaneously in the wave packet interaction. Special attention was paid to the complex 3D linear interactions which might precipitate large amplitudes even when the amplitudes of the individual, non interacting perturbations are small.

The project was subdivided into three intermediate steps consisting of: (i) an experimental and theoretical investigation of a single harmonic disturbance originating from a point; (ii) an interaction of two harmonic disturbances displaced in the spanwise direction and (iii) a calculation simulating an interaction of two harmonic disturbances displaced in the streamwise direction.

Linear Theory

Consider the 3D disturbance to be of the familiar form:

$$u_j(X,Y,Z,t) = u_j(Y)\, e^{i(\alpha X+\beta Z-\omega t)} \qquad (1)$$

where $j = 1,2,3,4$ corresponds to the three components of velocity u, v, w, and pressure fluctuations respectively and substitute it into the linearized equations of motion. The result is a set of equations derived in Ref. 12:

$$\left(\frac{d^2}{dy^2}-\kappa^2\right)^2 v - i\alpha R_{\delta^*}\left\{(U-c)\left(\frac{d^2}{dy^2}-\kappa^2\right)-\frac{d^2U}{dy^2}\right\} v=0 \qquad (2.1)$$

$$\left[\frac{d^2}{dy^2}-\kappa^2 - i\alpha R_{\delta^*}(U-c)\right]\zeta_y = i\beta R_{\delta^*}\frac{dU}{dy}\, v \qquad (2.2)$$

$$u = \frac{i}{\kappa^2}\left(\alpha\frac{dv}{dy} - \beta\zeta_y\right) \qquad (2.3)$$

$$w = \frac{i}{\kappa^2}\left(\beta\frac{dv}{dy} + \alpha\zeta_y\right) \qquad (2.4)$$

Equation (2.1) represents the 3D equivalent of the Orr-Sommerfeld (OS) equation from which both v and the eigen values α,β can be calculated. The vertical vorticity component ζ_y which appears in equations (2.1-4) is given by:

$$\zeta_y = \frac{\partial u}{\partial z} - \frac{\partial w}{\partial x} \qquad (3)$$

and therfore equation (2.2) is referred to as the vertical vorticity equation. In the spatial case α, is complex while ω and β are real.
The boundary conditions for the OS equation are:

$$v = \frac{dv}{dY} = 0 \quad \text{at} \quad Y = 0, \infty \qquad (4.1)$$

and for the vertical vorticity equation:

$$\zeta_y = 0 \quad \text{at} \quad Y = 0, \infty \qquad (4.2)$$

In this context it is worth noting that the well known Squire transformation (Ref. 11) is commonly interpreted to imply that every 3D normal mode has an equivalent 2D normal mode, existing at a lower Reynolds number. However, this simplified assumption is not always helpful, since certain combinations of frequency, Reynolds number and wave orientation, may actually lead to higher 3D amplification rates.

The 3D Orr-Somerfeld equation was solved numerically by using a shooting procedure described in detail elsewhere (Ref. 13, for a solution of the 2D case). Proper changes have been implemented in the above procedure for the integration of the full 3D equation (i.e Eq. 2.1-4). For a convenient comparison with experiment, the complex eigen functions are represented by an amplitude and a phase:

$$|u| = \sqrt{Re(u)^2+Im(u)^2},\quad \phi = tg^{-1}\left[\frac{Im(u)}{Re(u)}\right] \qquad (5)$$

Numerical Prediction of the HPS Maximum Amplitude

The normal mode representation of a three dimensional, small amplitude, harmonic disturbance has the following form (Ref. 7):

$$X^{-0.25}\,\mathrm{Exp}\left\{ i\left[\int_{X_S}^{X} \alpha dX + \beta Z - \omega t \right] \right\} \qquad (6)$$

where $X^{-0.25}$ is a factor that accounts for the effect of the boundary layer divergence. Mack (Ref. 7) proposed a similar expression for the amplitude of the streamwise component of the velocity fluctuations:

$$u(X,Z,t,\omega) = \mathrm{Exp}(i\omega t) \int_{-\infty}^{\infty} \mathrm{Exp}\, i\phi(\beta,X,Z)\, d\beta \qquad (7)$$

and for the complex phase:

$$\phi(X,Z) = \int_{X_S}^{X} \alpha(X;\beta,\omega)\, dX + \beta Z \qquad (8)$$

where α is the complex eigen value obtained from the 3D OS equation and the spanwise location of the source is at Z_p=0. This model, like the previous one (Ref. 7), also ignores the shape of the eigen functions.

The numerical scheme used presently for calculating the evolution of the HPS disturbance contained the following steps:

1) The eigen values of the spatial 3D OS equation (Eq. 3.4) were calculated for the Blasius velocity profile in the range of $700 < R_{\delta^*} < 1200$ at increments of $R_{\delta^*} = 25$. The inclination of the wave crests relative to the Z axis varied from 0-70° at 1° increment. Advantage was taken of the anti-symmetry in β.
2) Calculation of the amplitudes and the phases over the entire region considered in the experiment i.e. for $700 \le R_{\delta^*} \le 1200$ and $|Z_S / X_S| < 0.3$.

Experiment

The evolution of a single wave train and the interaction between two wave trains emanating from separate sources, located in a Blasius boundary layer and displaced in the spanwise direction, were investigated experimentally. The experiment was conducted in the close loop, low turbulence wind tunnel at Tel-Aviv university.

A fully automated, computer controlled experiment was constructed, which encompassed automatic hot-wire calibration procedure and probe traversing in the proximity of the wall. A polished aluminum plate 19 mm thick and 2.5 m long was installed vertically in the 10' long removable test section. The plate has an elliptic leading edge and a trailing-edge flap in order to control the circulation around the plate and through it the location of the leading-edge stagnation line. The turbulent corner flow originating at the juncture of the plate and the side walls was forced to bleed to the backward side of the plate through adjustable slots. This was achieved by a slight increase in the static pressure on the working side of the plate which helped to maintain a long fetch of laminar flow on that surface. The free stream velocity was maintained at 7.5 m/s throughout. The calculated Reynolds number based on the measured displacement thickness agreed with the expected values for the Blasius boundary layer as shown in figure 1.

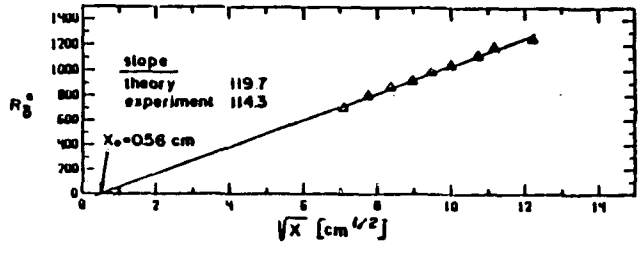

Fig. 1 R_δ^* vs $\sqrt{X}$

The spanwise distribution of R_{δ^*} in the region of interest was maintained at its nominal value by 5%. The top and bottom walls of the test section were adjusted until the measured Falkner-Skan Parameter (FSP) vanished, or at least did not exceed the value ±0.05 which was the possible resolution of the measurement. The FSP is a very important parameter strongly affecting the critical Reynolds number and the linear amplification factor.

Controlled harmonic disturbances were generated by two miniature hearing-aid earphones embedded on the rear side of the flat plate and ejecting tiny jets of air through 0.5 mm holes. These sources were located 50 cm from the leading edge of the plate, corresponding to R_{δ^*} = 700. The spanwise separation between the two sources was 80 mm which was equivalent to approximately 50 local displacement

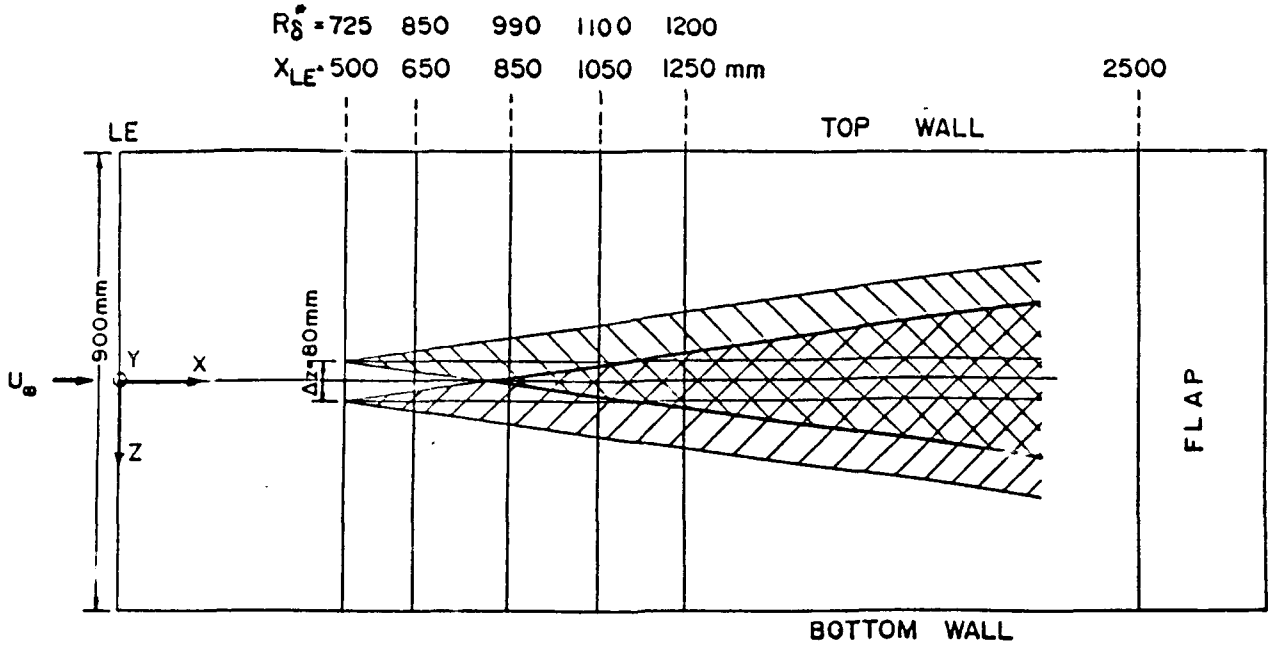

Fig. 2 Flat plate apparatus, spreading rate of the two HPS disturbances and overlap regions.

thicknesses at the free stream velocity of 7.5 m/sec and amounted two wave lengths of a typical perturbation at the dimensionless frequency of F=104. Both sources were activated by the same input signal and their output amplitudes were matched in order to produce equal amplitudes at any desired phase shift.

The disturbances from a single harmonic-point-source spread in the spanwise direction at half an included angle of 8-10°, consequently the prescribed spanwise separation between the sources allowed each wave train to develop independently before it overlapped and interacted with its neighbor (see Figure 2). The interaction experiment was done in three steps. In the first step both sources operated simultaneously while subsequently each source operated alone under identical flow conditions. In this way, any residual asymmetry in the flow or any uncontrollable perturbation in the tunnel would affect all three stages of the experiment equally and could be subtracted out. The amplitude and phase distributions of the streamwise component of the velocity fluctuation were calculated from data sampled across the entire boundary layer at every X,Z location. More than 30 points of the streamwise velocity component were measured within the boundary layer between the wall and and the Y location corresponding to $4\delta^*$. The maximum amplitudes presented were determined with respect to Y at every X,Z location while the phase reference was chosen at the location at which the amplitude was maximum (i.e Y_{ma}). The flow was interrogated along the center-plane of every isolated harmonic disturbance (i.e $Z=Z_p$), along the center-plane of the combined disturbance (i.e. at Z=0) and across the entire span of the disturbance at a few select R_{δ^*} stations. The effect of constant phase mismatch between the two harmonic disturbances was documented in order to study the outcome of such a mismatch hoping to achieve a favorable interaction and possibly a suppression of this type of disturbances. The two harmonic sources were operated at almost equal amplitudes but at a phase differences of 0, $\pi/2$ and π.

Results and Discussion

The evolution of an isolated harmonic point-source disturbance

The shape of the amplitude and phase distributions vs Y of the velocity fluctuations change along the span of the HPS, implying that there is a concomitant change in the form of the eigen function along the span, in contradistinction to the 2D case. The amplitude and phase distributions measured directly downstream of the single source (i.e. at $Z=Z_p$) agreed very well with the eigen functions calculated for the purely 2D case (Figure 3a).

This is not surprising, because symmetry requirements dictate that the dominant wave on the center-plane must be two dimensional (i.e. $\beta=0$), as demonstrated on the top portion of figure 4. The spanwise distribution of the maximum amplitude and the phase shift measured at the Y location at which the maximum amplitude occurs relative to its occurrence on the plane of symmetry are plotted on the lower part of figure 4. The solid lines, in this figure, represent the best fit to the data. The spanwise wave number becomes infinitely large toward $Z_p=0$ and $\beta\delta^*$ is anti-symmetrical with respect to the centerline, on which it is suppose to vanish implying that the disturbance is two dimensional there. Away from the center-plane (e.g. on the ray $Z_s / X_s=0.136$), where the oblique waves are dominant and $\beta\delta^*=0.2$, the experimentally determined eigen functions are quite different (Figure 3b). The calculated phase and amplitude distributions of the u component of the velocity perturbation for $\beta\delta^*=0.2$, F=104, and $R_{\delta^*}=1100$ are in excellent agreement with the measured data. Similar agreement was found at other frequencies and spatial locations, as it is demonstrated by the results presented in figure 5. It should be mentioned that the data is normalized whereupon the maximum amplitude and one point in the phase distribution are matched with the calculated values. An increase in the forcing amplitude did not cause measurable distortions of the eigen functions or a noticeable change in the amplification rate provided the forcing amplitude was less than 3% of the free stream velocity (or a local amplitude of 1% further downstream).

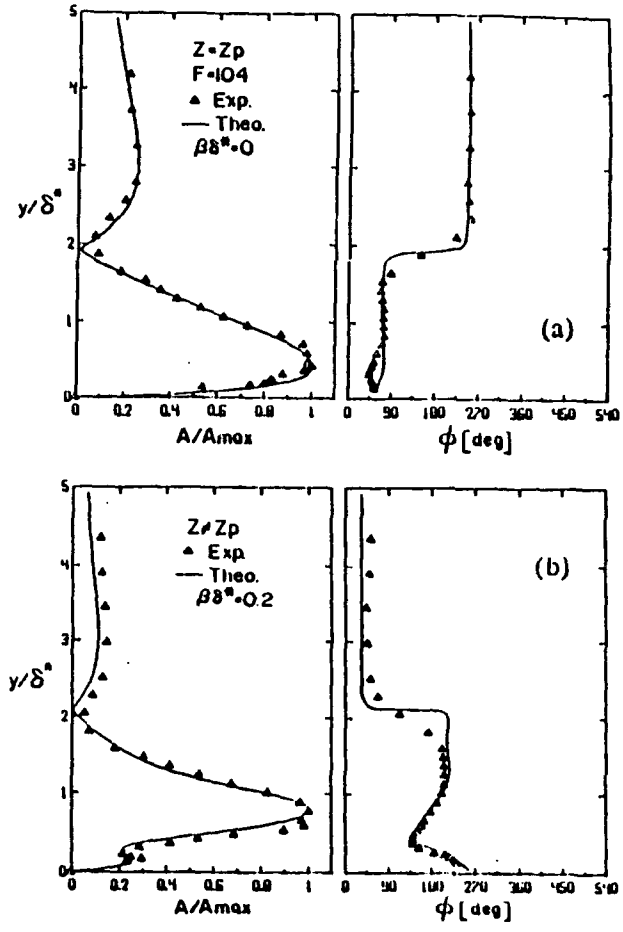

Fig. 3 Measured and calculated eigen functions on (a) and off-centerline (b), F=104 at $R_{\delta^*}=990$ ($X_s=35$ cm)

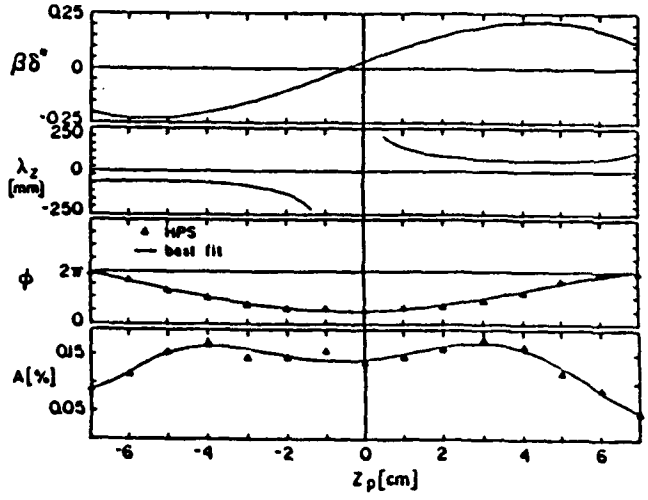

Fig. 4 Experimental HPS spanwise wavenumber, wave length, phase and maximum amplitude vs Z, F=104 at $R_{\delta^*}=990$ ($X_s=35$cm).

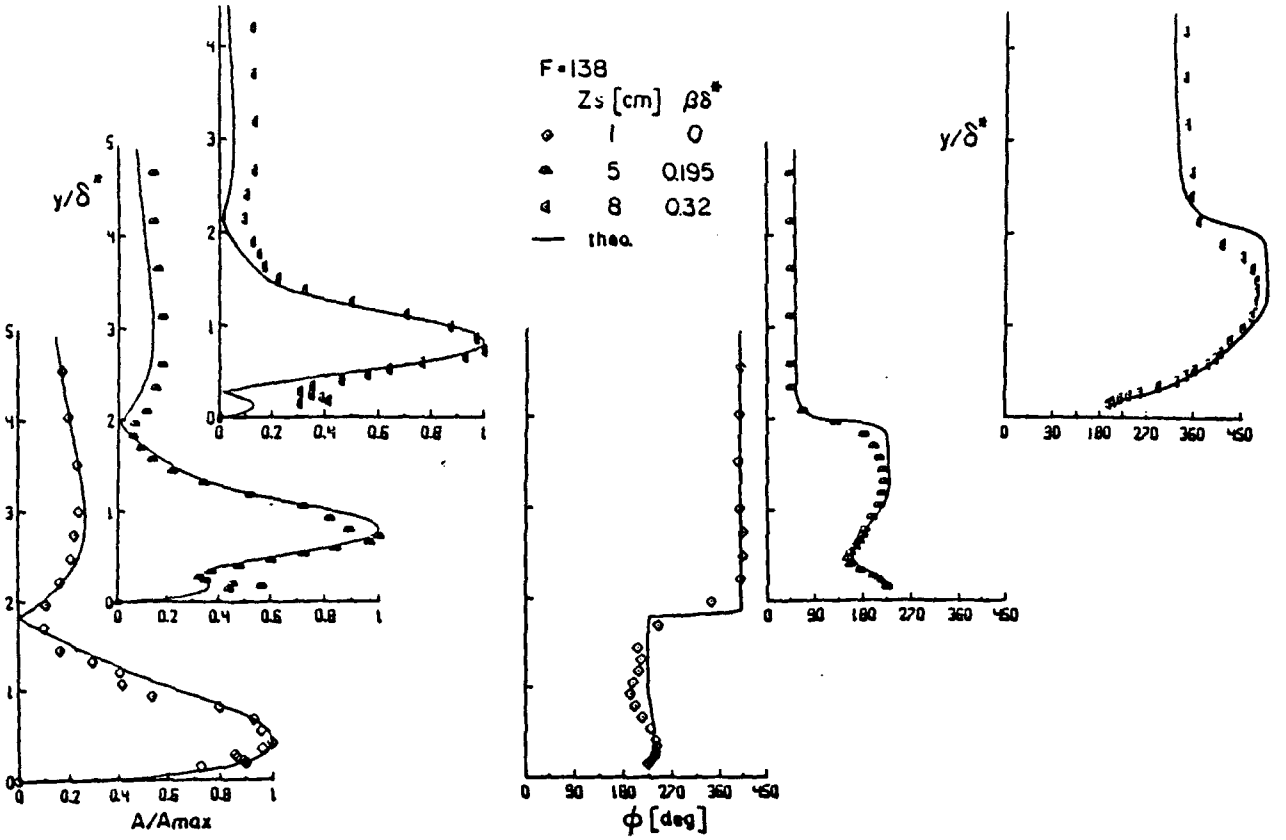

Fig. 5 Comparison between measured and calculated eigen functions on and off-centerline, F=138 at R_{δ}*≈990.

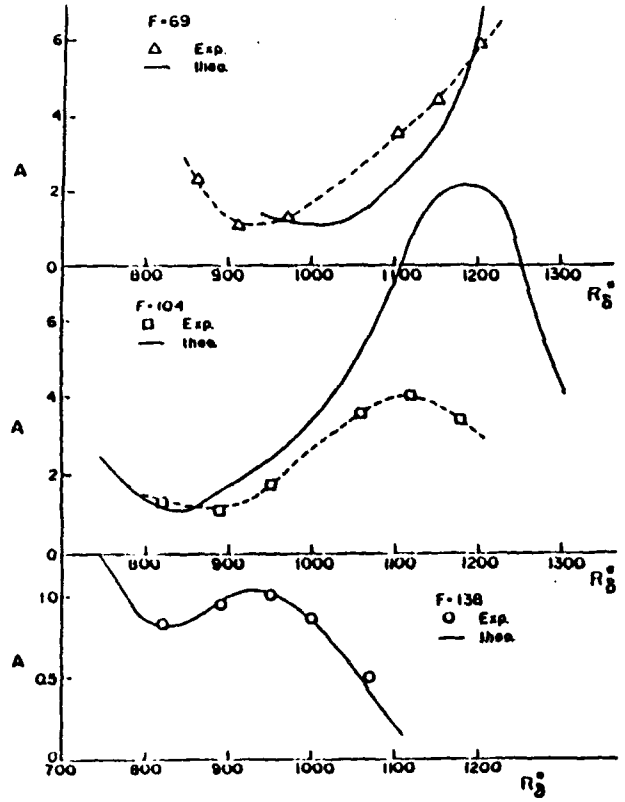

Fig. 6 Normalized maximum amplitudes vs R_{δ}* for F=69, 104 and 138, comparison between experiment and theory.

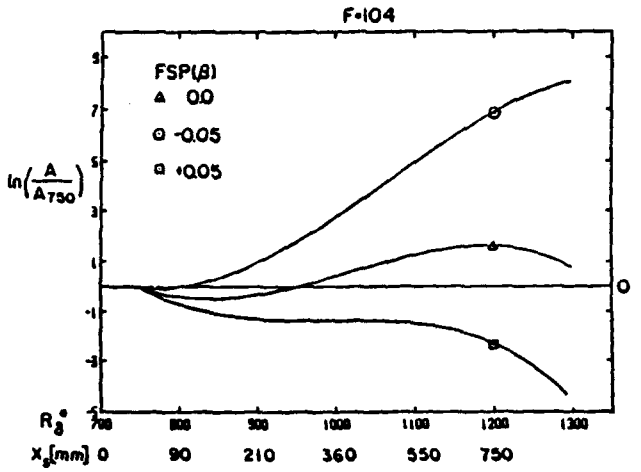

Fig. 7 Calculated HPS maximum amplitudes vs R_{δ}* on Z_s=0, F=104, for Falkner-Skan parameters of -0.05, 0 and 0.05.

A comparison between the measured and the calculated, maximum amplitude distributions on the plane of symmetry, for a variety of dimensionless frequencies, is made in figure 6. The calculations are based on Mack's model and are in fair agreement with the experimental observations.

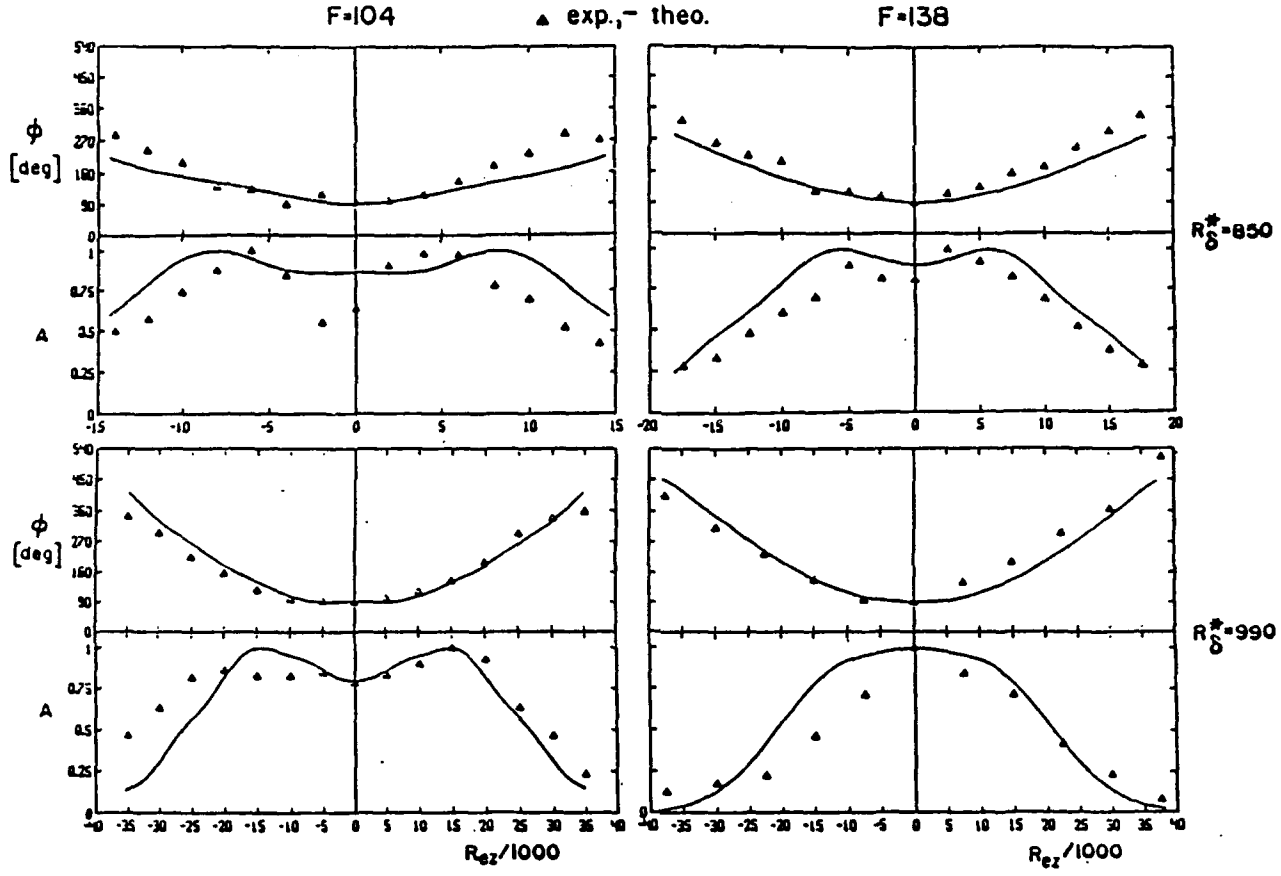

Fig. 8 Comparison between experimental and theoretical maximum amplitude and phase at $Y=Y_{ma}$ vs Z at R_{δ}^{*}=850 and 990, F=104 and 138.

When assessing the quality of this comparison one should consider the tremendous sensitivity of the measured amplification rate to pressure gradients. The streamwise amplification of a dominant harmonic disturbance is presented in figure 7 for the range of distances used in the present experiment. The three curves shown correspond to different Falkner-Skan parameters, ranging between ±0.05 values. It should be remembered that the difference between a velocity profile corresponding to a FSP of 0.05 and of 0 is hardly discernible experimentally, yet the differences in the integrated amplification rate over the distances considered presently may result in amplitudes which are orders of magnitude apart. Consequently the disparity between theory and experiment shown in figure 6 is insignificant. The sensitivity of the streamwise amplification to pressure gradient dissuaded us from refining the theoretical model by including in it the slight, streamwise divergence of the laminar boundary layer.

Spanwise amplitude and phase distributions, corresponding to the Y location at which the amplitude is maximum were also calculated using Mack's model. A sample of these calculations is compared with experimental data (Figure 8) for two streamwise locations (R_{δ}^{*}=850 and 990) and for two dimensionless frequencies (F=104 and 138).

It should be noted that the spanwise amplitude and phase distribution depends on the distance from the source, on the frequency and on the streamwise location of the source itself. It is anticipated therefore, that only a local and partial suppression of the wave can be achieved by the destructive spanwise interaction between two, locally concentrated, harmonic disturbances.

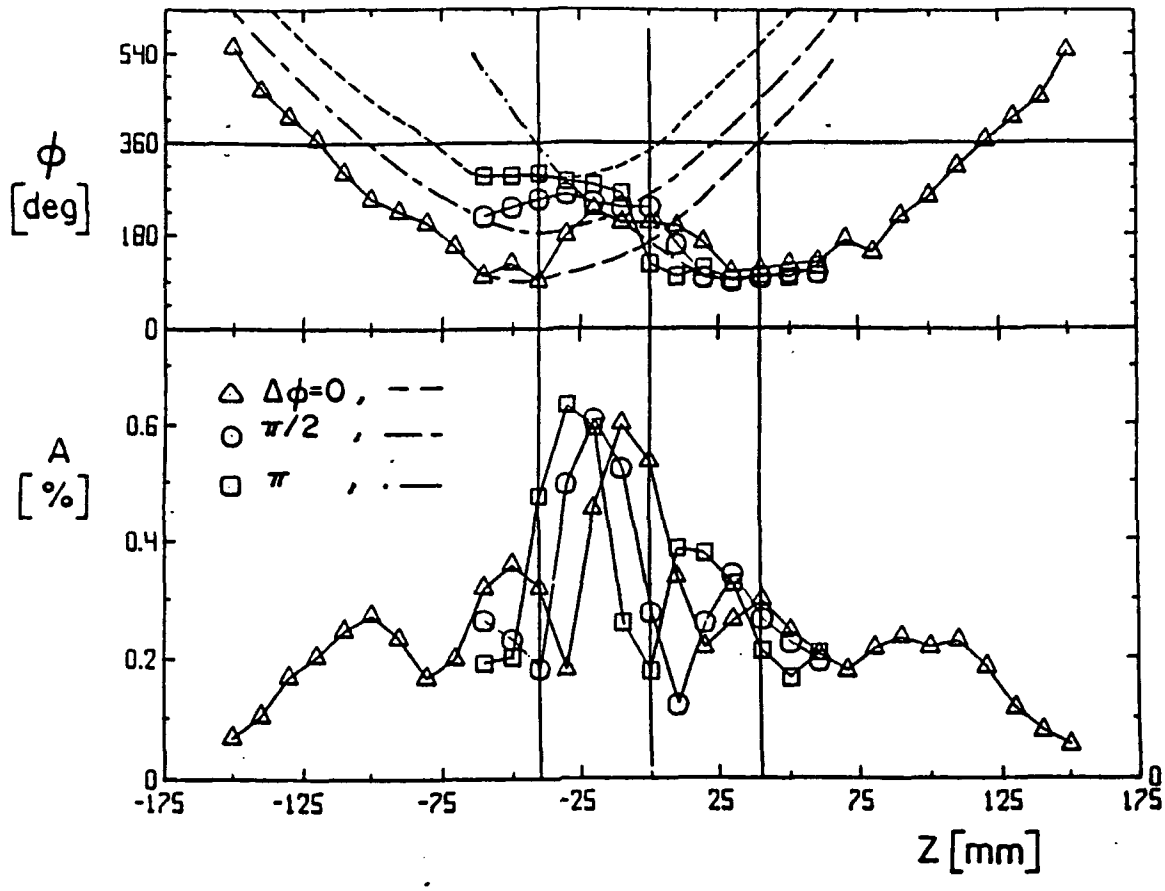

Fig. 9 THPS MA and phase at $Y=Y_{ma}$ vs Z, at phase differences of $\Delta\phi=0$, $\pi/2$ and π, $R_\delta^*=1100$ (X_s=55cm).

Spanwise interaction

Three spanwise distributions of the maximum amplitudes observed at a given streamwise location are plotted in figure 9 together with their respective distribution of phase-angles. These results were obtained while the two spanwise separated point-sources of harmonic disturbances were operating simultaneously, at almost equal amplitudes.The phase difference between the sources was controlled and the data presented corresponds to three principle phase differences of 0, $\pi/2$ and π radians.

One may observe from this illustration that the initial phase difference does not affect the maximum amplitude attained at some arbitrary X,Z location in the boundary layer. The control of the phase-shift between the harmonic disturbances can only displace the location at which the maximum amplitude occurs along the span but not suppress this amplitude. This is not surprising when one takes into consideration the steep spanwise phase gradients occurring downstream of an isolated, harmonic-point-source disturbance.

The perturbation resulting from such two interacting disturbances may be effectively reconstructed from the data collected for each isolated disturbance, by a linear superposition, provided that the shape of the eigen function at every X,Z location is known and the spanwise separation and phase shift are taken into consideration. In order to form a correct linear superposition of the two disturbances, one should sum up the two complex eigen functions acquired at the same X,Z location, in the form

$$\Psi_{sup}(y) = A_1 e^{i\phi_1} + A_2 e^{i\phi_2} \qquad (9)$$

A_1, A_2, ϕ_1 and ϕ_2 are functions of Y. The superimposed signal should be compared with the ensuing disturbance generated by the two harmonic point-sources (THPS) operating in unison. Any deviation of the measured amplitude or phase of the disturbance during the THPS experiment from the results calculated by superposing the perturbations generated by HPS could be attributed to non-linear effects. An example of such a summation is given in figure

10 (for F=104 at R_{δ}*=1100 and Z=0). The upper part of this figure presents the two isolated HPS disturbances participating in the interaction while the lower part shows the measured THPS disturbance in comparison to the calculated linear superposition.

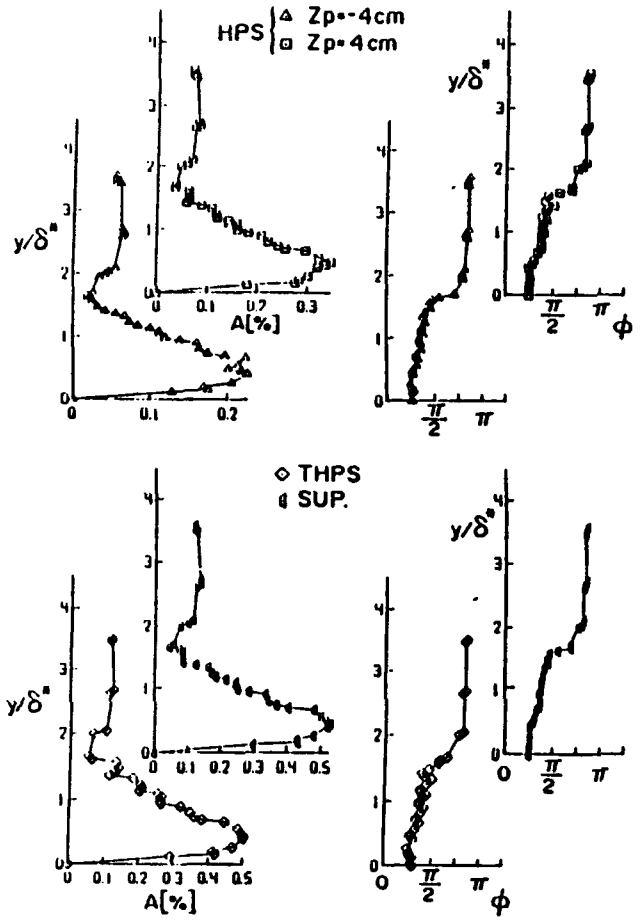

Fig. 10 Two experimental HPS eigen functions, their linear superposition and the THPS eigen functions for the same case, F=104, R_{δ}*=1100 (X_s=55cm), all on Z=0.

It can be concluded, on the basis of the very good agreement observed in figure 10, that a linear superposition is permissible within the range of parameters considered. The validity of this technique is also demonstrated in figure 11 (for F=104 and at R_{δ}*=990) for the spanwise distribution of the disturbance. In this case, a simple reflection technique, with respect to the plane of symmetry (i.e Z=0 in fig. 2), was used.

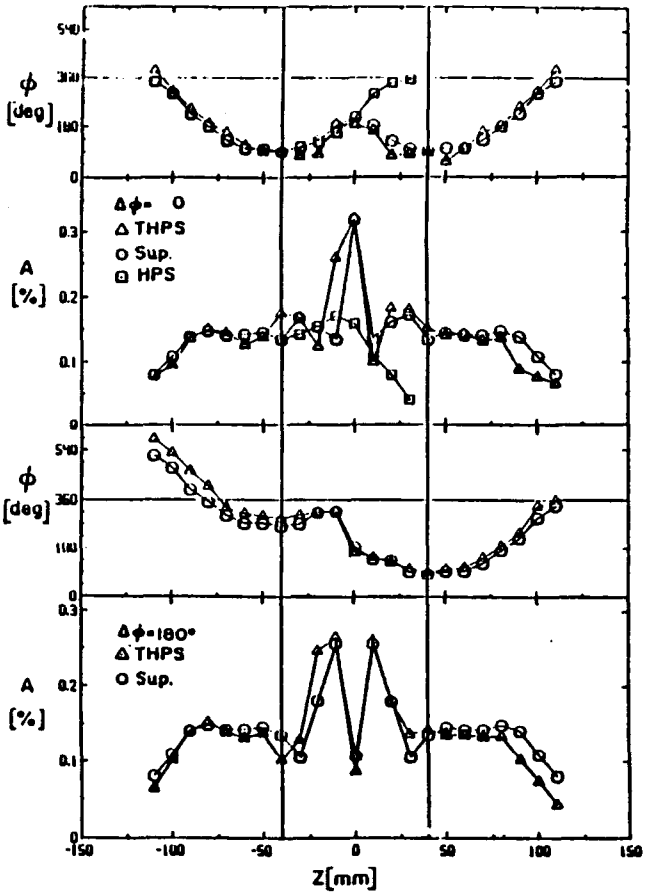

Fig. 11 Comparison between THPS and the linear superposition of the two HPS at phase shifts of $\Delta\phi$=0 and π/2.

The resemblance between the reconstructed and measured amplitudes and phases of the perturbations is satisfactory. The comparison shown in figure 11 is applied to other phase shifts between the original sources with equal success. Some of the observed differences may stem from the imperfections in the assumed symmetry of the laminar boundary layer.

Streamwise Interaction

Having established the validity of the linear superposition, between two experimentally measured harmonic wave trains introduced at the same X (i.e. the same $R_\delta*$) while being separated along the span, encouraged us to expand the numerical scheme to include other possible spatial interactions. We thus considered the interaction of two equal frequency (F=104) wave trains, originating from point-sources located in tandem (one downstream of the other) at $R_\delta*$=700 and 800. It should be emphasized that the calculated patterns of amplitude and phase are only representing the Y location at which the amplitude is maximum and neglect the changes in the shape of the eigen functions occurring along the span. The validity of these results is also limited to the lower amplitudes of the ensuing disturbance, thus assuring linear behavior. The calculated amplitude and phase distributions of the two isolated HPS disturbances are plotted vs R_{ez} in Figure 12. In the chosen example, the two superimposed wave trains originated from point-sources located at $R_\delta*$=700 and 800 respectively, while the resulting disturbance is calculated and presented at $R_\delta*$=900.

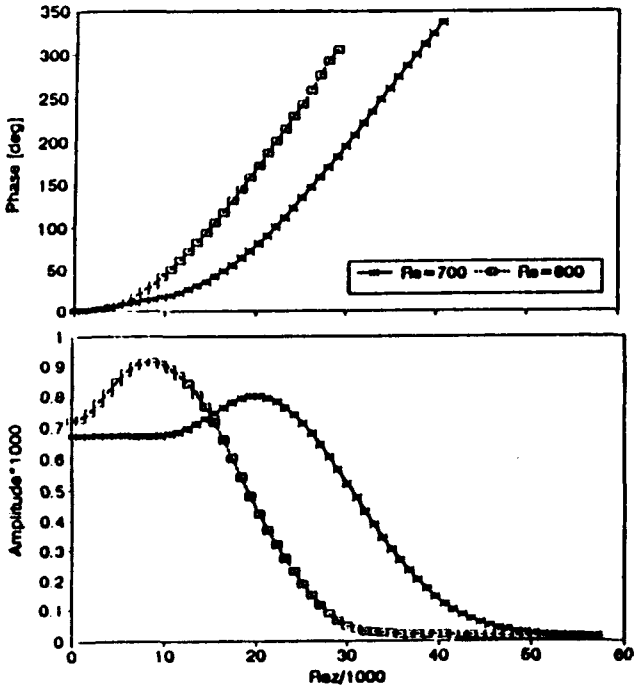

Fig. 12 Calculated amplitude and phase distributions for two isolated HPS originating at $R_\delta*$=700 and 800 and presented at $R_\delta*$=900.

The individual amplitudes of each source were approximately equal on the centerline (figure 12) at $R_\delta*$=900 but the normalized spanwise distribution of the amplitude depended on the distance from the source and on the $R_\delta*$ at the source. The result of the superposition is shown in Figure 13 for three relative phases of the disturbance on the centerline, namely $\Delta\phi$=0, $\pi/2$ and π. It is clear that only a local suppression of the harmonic disturbance is feasible in spite of the fact that the relative choice of the amplitudes is arbitrary. When complete cancellation is attained on the plane of symmetry the result at R_{ez} greater than 25,000 is not affected by the interfering wave. One may continue the computation of the interacting wave trains to other streamwise locations (Fig. 14) and observe that the amplitude-peak moves away from the plane of symmetry with increasing X.

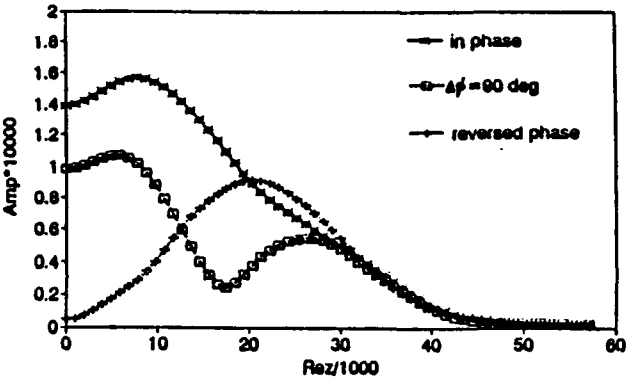

Fig. 13 Calculated amplitudes of a linear superposition of the two isolated HPS disturbances presented in Fig. 12 at three relative centerline phases.

The effectiveness of this suppression is measured by comparing the ensuing amplitudes to the amplitudes existing in the flow without interference (i.e. amplitudes produced by an isolated harmonic point-source disturbance). In the present example an attempt was made to suppress a disturbance originating at $R_\delta*$=700 by another disturbance located directly downstream at $R_\delta*$=800, while the results were observed at various spanwise locations between $R_\delta*$=850-1050. Even the most effective suppression (occuring at $\Delta\phi=\pi$) resulted initially (at $R_\delta* < 1000$) in absolute amplitudes along the span which were higher than the amplitude produced by a single HPS. Further downstream, the interference is favorable and the combined amplitude of the perturbation is lower than for

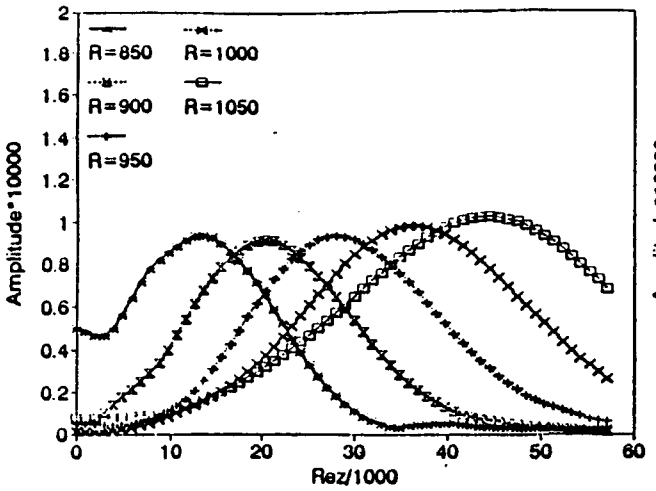

Fig. 14 Calculated amplitude vs R_{ez} of streamwise THPS interaction (originating at R_{δ}*=700 and 800) plotted at various downstream ($R=R_{\delta}$*) stations.

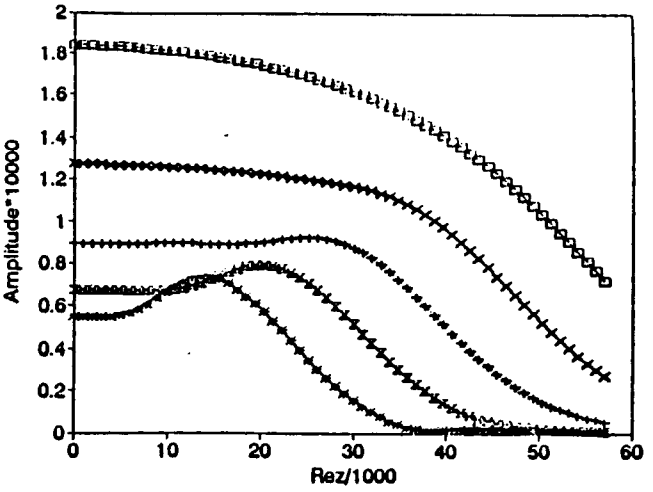

Fig. 15 Calculated amplitude vs R_{ez} of an isolated HPS interaction (originating at R_{δ}*=700) plotted at various downstream ($R=R_{\delta}$*) stations. Symbols similar to Fig. 14.

an isolated HPS (fig 15). The rise in the initial amplitude of the combined disturbance at short distances from the secondary source may introduce non-linear effects which were not considered presently and consequently the eventual suppression predicted for $R_{\delta}^* \geq 1000$ may not materialize.

Conclusions

It was confirmed experimentally that the evolution of a single, harmonic, point-source disturbance, in a boundary layer is well predicted by a linear model. Furthermore, the spatial interaction of two or more such low amplitude disturbances, can be modelled by linear superposition in spite of the complicated phase relationships existing among such disturbances. This simplification enables one to predict the net effect of any desired distribution of point-source disturbances, as long as the resulting amplitudes remain low.

The total suppression of a harmonic, three dimensional, disturbance within a short streamwise distance from its detection is virtually impossible to achieve unless one contemplates a distributed control mechanism consisting of large number of individually activated sources of perturbation. This conclusion should also be valid for the impulsively generated three dimensional wave-packet because its spanwise structure consists of Fourier components, which are individually identical to the harmonic-point-source disturbance (Ref. 14).

Acknoledgements

This project was supported in part by a grant from the United States Air Force (AFOSR 89-0307) and monitored by Dr. J. McMichael.

Refrences

1. Kachanov, YU.S., Development of spatial wave packet in boundary layer, proceedings of the IUTAM symposium on Laminar-turbulent transition, Novosibirsk 1984, Ed. Kozlov, V.V., p. 115.
2. Mack, L.M. and Kendall, J.M., Wave patterns produced by a localized harmonic source in a Blasius boundary layer, 1983, AIAA paper 83-0046.
3. Wehrmann, US patent number 3,362,663, 1968.
4. Liepmann, H.W., Brown, G.L. and Nosenchack, D.M., Control of laminar -instability waves using a new technique, J. Fluid Mech., 1982, vol. 118, p. 187.
5. Thomas, A.S.W., The control of boundary layer transition using a wave superposition principle, J. Fluid Mech., 1983, vol. 137, p. 233.
6. Pupator, P.T. and Saric, W.S., Control of random disturbances in a Boundary Layer, Abstract submitted to the 2nd shear flow control conference, 1989.
7. Gaster, M., A Theoretical Model for the development of a wave packet in a laminar boundary-layers, 1975, Proc. Roy. Soc. Lond., A. 347, P. 271.

8. Gaster, M. and Grant, I., An experimental investigation of the formation and development of a wave packet in a laminar boundary layer, 1975. Proc. Roy. Soc. Lond., A. 347, P. 253.
9. Benjamin, T.B., The development of three dimensional disturbances in an unstable film of liquid flowing down an inclined plane, J. Fluid Mech., 10, 1961, p. 401-419.
10. Criminale, W.O. and Kovasnay, L.S.G., he growth of localized disturbances in a laminar boundary layer, J. Fluid Mech., 1962, 14, p. 59.
11. Squire, H.B., On the stability of three-dimensional disturbances of viscous flow between parallel walls, Proc. Roy. Soc. Lond., 1933, A. 142, p. 621.
12. Benny, D.J. and Gustavsson, L.H., A new mechanism for linear and nonlinear hydrodynamic instability, Stud. in App. Math., 1981, 64:185-209.
13. Katz, Y., On the evolution of a turbulent spot in a laminar boundary layer with a favorable pressure gradient, PhD thesis, 1987, Tel-Aviv Uni.
14. Seifert, A., On the interaction of low amplitude disturbances emanating from discrete points in a Blasius boundary layer, PhD thesis, 1990, Tel-Aviv Uni.

APPENDIX B

Active Control of Skin Friction and Separation in Certain Class of Wall-Bounded Flows

by I Wygnanski

ACTIVE CONTROL OF SKIN FRICTION AND SEPARATION IN CERTAIN CLASS OF WALL-BOUNDED FLOWS

presented by:

I. Wygnanski

Department of Aerospace Engineering University of Arizona
and
Department of Fluid Dynamics & Heat Transfer
Tel Aviv University

ABSTRACT

Experimental investigations of large coherent structures in turbulent shear flows bypassed the boundary layer in the presence of a strong, adverse-pressure-gradient and the wall-jet. Both are wall bounded flows having one characteristic in common: their mean velocity profile is inviscidly unstable to two dimensional perturbations. Thus the identification of the large coherent structures with the predominant instability modes might be extended to this class of flows and could be quantitatively analyzed. The apparent similarity between the wall-jet and a combination of a free jet and a boundary layer is explored was and the relevance of the solid surface to the evolution of the large coherent structures was assessed. From this point of view, the boundary layer in a strong adverse pressure gradient, is regarded as a wake evolving in the vicinity of a solid surface. In both flows the significance of the outer region is accentuated while the no-slip conditions at the solid surface are maintained.

The response of these flows to external, two dimensional excitation is currently being investigated in an attempt to further the understanding of the interactions between the inner and the outer structures in a turbulent boundary layer. While doing so, two technologically important effects were discovered. The mean flow in the wall wake remained attached in spite of the strong adverse pressure gradient which caused separation in the absence of the excitation while the skin friction in the wall jet was reduced as a consequence of the excitation.

INTRODUCTION

Investigations of large coherent structures in turbulent shear flows concentrated either on wall bounded flows like a boundary layer or a channel[1,2] or on free shear flows like the mixing layer, the wake and the jet[3-5]. In the latter category of flows, the large coherent structures were clearly identified as the predominant instability modes and were quantitatively analyzed in this context. In fact, one may formally show that the coherent eddies existing in a two-dimensional, turbulent, mean flow are, to a first approximation, governed by the Orr-Sommerfeld equation provided one decomposes the equations of motion into coherent and incoherent motion[6], one neglects the second order products of both motions and one restricts the divergence of the mean flow. The triple decomposition, therefore, enables one to link the hydrodynamic stability analysis with quantitative definitions of coherent structures.

However, the large coherent structures in wall bounded flows are much more complex and more difficult to identify then in free shear flows. Many forms of such structures were observed visually[7,8] but no consensus was reached as to their origin and their precise association with the enhancement of the skin-friction or with the rate of growth of the boundary layer. Since Hussain and Reynolds[9,10] failed to excite growing two-dimensional modes in a turbulent channel flow, it was tentatively concluded that plane instability modes are not related to the large coherent structures observed in channels and boundary layers. However, instabilities akin to the ones

responsible for the generation of hair-pin vortices in a laminar boundary layer[11], may still be identified with the creation of large coherent structures in fully turbulent wall bounded flows. In fact "sublayer streaks" were recently modelled by Landahl[12], by using an instability concept associated with three dimensional intermittent disturbances growing algebraically in the direction of streaming.

Free shear flows are inviscidly unstable, while boundary layers in the absence of an adverse pressure gradient are not (figure 1). There is enough evidence[13] to suggest that a boundary layer on the verge of separation resembles a free mixing layer and it responds to external stimuli, like a mixing layer. The receptivity of this boundary layer is attributed to an inviscid instability which may dwarf any other form of instability and generate large, predominantly two-dimensional, coherent structures. The wall jet is inviscidly unstable (figure 1) in its outer region and may thus possess large coherent structures characteristic of a plane turbulent jet. The wall jet might be the ideal flow configuration for resolving the intricate interactions between the outer and the inner structures in a turbulent boundary layer, because it offers a larger degree of flexibility and controllability of flow parameters than a boundary layer does, regardless of pressure gradient. This flexibility stems from the fact that, the vorticity in the outer layer depends on the added momentum flux which for a given free stream and jet efflux velocity depends also on the dimension of the nozzle. Thus the susceptibility of the wall jet to external perturbations might also depend on the ratio between the wave-length of the perturbation, the width of the nozzle and the upstream boundary layer thickness. Consequently the structure of the wall jet can be progressively altered and the importance of the outer vortical layer on the wall region, can be evaluated.

The boundary layer in a strong adverse pressure gradient, may be regarded as a wake adjacent to a solid surface and might be subjected to the same kind of stability analysis. In both flows the significance of the outer region is accentuated while the no-slip conditions at the solid surface are maintained. The vorticity near the surface of the wall-jet has an opposite direction to the vorticity in its outer layer and may detract from its strength. On the other hand, the vorticity near the surface of the wall-wake may reinforce the vorticity in its outer region. The superposition of an external stream on the wall-jet weakens the vorticity in the outer region until it resembles a turbulent boundary layer in the limit.

Although one has less flexibility with the wall-wake than with the wall-jet in an external stream, the understanding of the former flow is technologically very important. In particular, the control of the large scale eddies in a turbulent boundary layer having a vanishingly small wall stress[14] might lead to a delay in boundary layer separation which is omnipresent in most flows around solid bodies. Preliminary observations associated with the wall-jet and wall-wake are presently discussed, stressing some features common to both flows. Many more measurements might be required before the concept is proven but the results obtained to date, are encouraging.

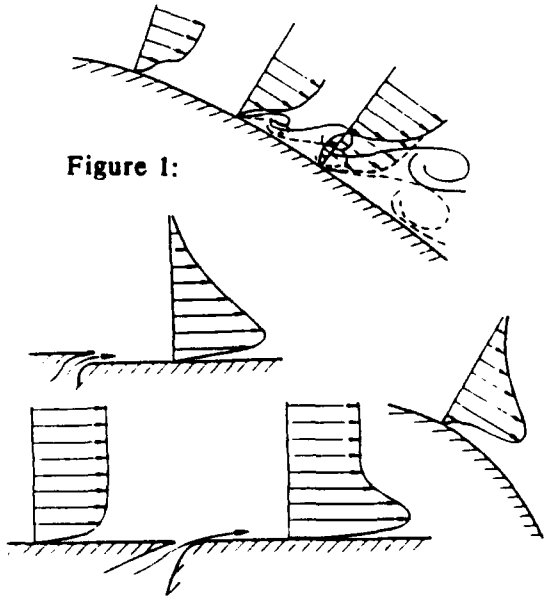

Figure 1:

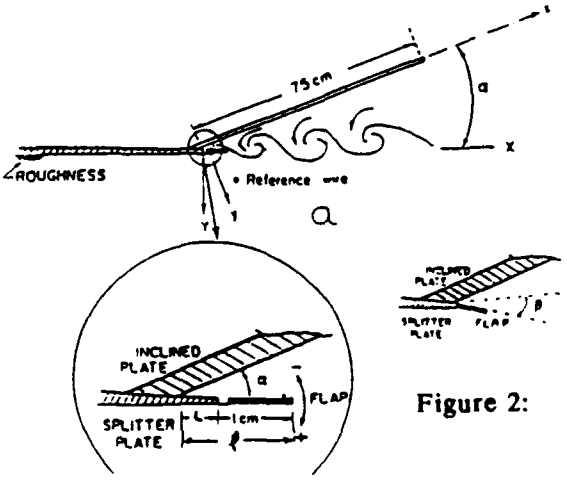

Figure 2:

A schematic of the wedge flow apparatus.

THE MEAN FLOW IN THE FORCED WALL-WAKE

The flow over a solid, convex wedge was investigated (figure 2). The wedge consisted of two long flat plates which were hinged together to provide a discontinuity in the slope of the surface and thus in pressure gradient. An 18° or a 22° wedge angles, which could not normally have been negotiated by the upstream boundary layer without separation, were used in the experiment. The different wedge angles depended on the detailed geometrical conditions at the discontinuity. A thin metal flap spanned the entire test section at the hinge location and, in the absence of the forced oscillations, the flow separated at its trailing edge. The surface of the splitter plate was roughend upstream in order to ensure that the boundary layer approaching the discontinuity was is thick, turbulent and two-dimensional. The velocity profiles measured are typical for a turbulent boundary layer in this range of Reynolds numbers (i.e., the shape factor $H \equiv \delta^*/\theta = 1.6$ for $Re_{\delta^*} = 800$). The maximum turbulent intensity, u'/U is approximately 7% 50 mm upstream of the hinge. The displacement amplitudes of the flap did not exceed ±1 mm. The imposed streamwise component of velocity oscillations were measured by a hot-wire located in the potential flow near the flap. The velocity perturbation was recorded together with the forcing signal, and the data were ensemble averaged in order to remove the free stream turbulence of the wind tunnel and other sources of random disturbances from contaminating the results.

The flow generated downstream of separation resembles the classical, unforced mixing layer observed in the absence of pressure gradient. The vorticity thickness, δ_ν, obtained by fitting a straight line to the mean velocity profile at the point of inflection[15] increases linearly with X, as it does in the classical mixing layer. The slope of the vorticity thickness $d\delta_\nu/dX = 0.23$ is in good agreement with previously made measurements in which the boundary layer on the splitter plate was tripped.[5] The pressure recovery coefficient $C_p \equiv (P - P_{init})/1/2\rho U^2_{init}$ was less than 0.1 over the distance of 60 cm because the flow was fully separated (figure 3).

Activating the flap at frequencies corresponding to Strouhal numbers based on initial momentum thickness $[St \equiv f\theta/U]_{init}$, which were smaller than 0.01 and reference amplitudes $u'/U_{init} > 0.25\%$, resulted in a reattachment of the flow to the surface and a pressure recovery of $C_p \equiv 0.5$ over the corresponding distance considered before (figure 3). The flow was partially reattached at reference amplitudes as low as 0.1%. One may conclude, therefore, that the externally introduced oscillations were sufficiently amplified to allow the boundary layer to overcome the adverse pressure gradient imposed by the divergence of the walls and the existence of the flap at the discontinuity.

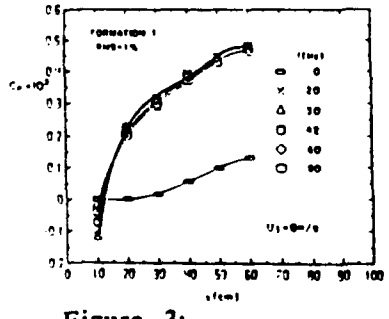

Figure 3:

The pressure distribution

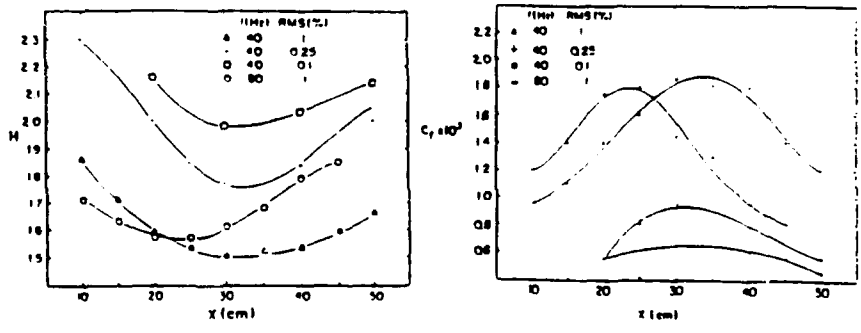

Figure 4: The variation of H and C_f with x

The dependence of some important boundary layer parameters, like the shape factor H, and the skin-friction coefficient C_f, on X is plotted in figure 4 for some of the frequencies tested and for the 3 amplitudes at a single frequency f = 40 hz. The momentum thickness increases almost linearly with X. The shape factor decreases initially with X and then gradually increases towards the trailing edge of the plate, while the skin friction coefficient behaves in an opposite fashion. The X location at which H is smallest corresponds to the location at which C_f is largest, as might have been expected from the momentum integral equation provided the pressure

increases monotonically with X. The location at which H has a minimum appears to depend primarily on the frequency of forcing and not on the amplitude, while the minimum value of H attained depends mostly on the amplitude of the imposed oscillations. The value of fX/U at which H attains its minimum is approximately 2, suggesting that the wave-length of the imposed oscillations determines the preferred reattachment distance.

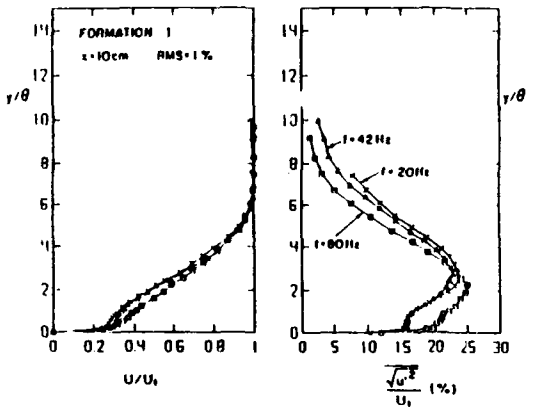

Figure 5:

Mean velocity and turbulent intensity profiles measured at x = 10 cms

Representative mean velocity and turbulent intensity profiles measured at X = 10 cm are plotted in figure 5 for three frequencies considered at a forcing amplitude of 1%. These profiles are typical of boundary layers at moderately adverse pressure gradients[16] with the exception of the maximum level of turbulence which exceeds 20% and is more characteristic of the level measured in separated flows.[17] When the mean velocity profiles are plotted in the usual "law-of-the-wall" coordinates the universal logarithmic distribution remains unchanged regardless of the forcing frequency or amplitude:

$$U^+ = 5.6 \log Y^+ + 5 \,. \tag{1}$$

The maximum value of Y^+ at which the equation applies depends not only on the pressure gradient but also on the amplitude and the frequency of forcing. It can be best correlated with the dependence of H on these parameters. The general representation of the "law-of-the-wake" also applies in all cases considered, i.e.,

$$W = C \sin^2\left[\Pi \frac{Y}{2\delta}\right] , \tag{2}$$

but the constant C depends on the frequency and amplitude of the forcing (fig. 6). It seems that in a "wall-wake" there is a large region in which the turbulent stress is approximately constant in contradistinction to the measurements done in a wall jet at moderate Reynolds numbers[18].

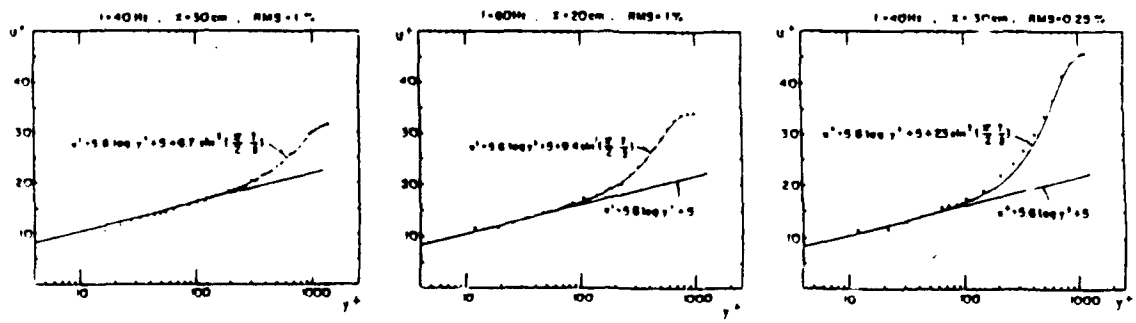

Figure 6: Mean velocity profiles plotted in the wall coordinates.

THE TRANSFORMATION OF THE WALL JET IN STREAMING FLOW TO A BOUNDARY LAYER

The experimental research was carried out in a low turbulence wind tunnel. The wall-jet originated from a two dimensional nozzle flush mounted into the floor of the tunnel in order to minimize its effect on the evolution of the boundary layer. The slot-width was altered by moving the entire front plate in the X-direction and inserting appropriate filling strips in the tunnel floor. The jet turns rapidly in the direction of streaming and the effects of its deflection could not be detected beyond 10 slot widths in most test conditions. The velocity was mostly measured in the developed region of the wall jet starting from 20 slot-widths downstream of the nozzle and extending sometimes beyond 200 slot-widths. The Reynolds number at the nozzle, Re_j, was altered by changing the efflux velocity, U_j, and the width of the slot, b. The ratio between the free stream velocity and the jet efflux velocity was also altered by varying the velocity in the tunnel, U_∞, and by varying U_j.

Typical streamwise evolution of mean velocity profiles are shown in fig. 7 where the top set corresponds to an initial velocity ratio $U_\infty / U_j = 0.085$, the central set to 0.59 and the bottom to 0.93. The effect of the upstream boundary layer is progressively stronger from top to bottom. These three sets of data were chosen because they may represent different categories of instability. The velocity profiles in the top data-set contain only one inflection point in the outer region. The outer region in this case resembles a free jet at all X locations. There are two inflection points in the outer region of the wall-jet near the slot of the second set, underlining the importance of the upstream boundary layer in this case. The relatively strong U_j overcomes this velocity defect whereupon downstream of the fourth station the mean-velocity profile no longer contains two inflection points. The effect of the upstream boundary layer is much stronger in the bottom set which resembles the development of a wake in the vicinity of a solid surface. Since the ratio of the free stream velocity to the jet velocity approaches unity near the nozzle the flow appears to relax directly to an ordinary boundary layer without passing through the intermediate stage of a wall-jet embedded in an external stream. **The wall jet in streaming flow may therefore represent the boundary layer in the limit.**

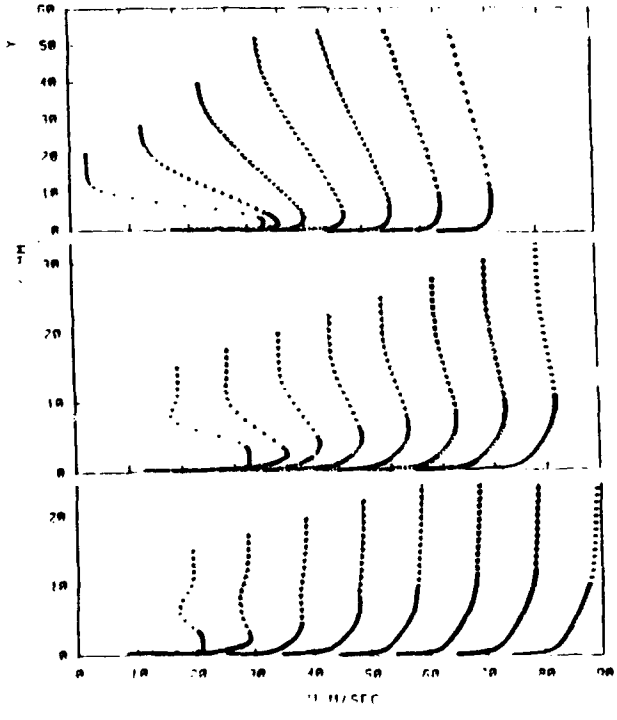

Figure 7: The evolution of a wall jet in an external stream

The attainment of similar mean velocity profiles is not essential in analyzing the evolution of the large coherent structures but it is very convenient because it enables one to reduce significantly the amount of computations and measurements required to prove the concepts outlined. It is well known that a complete self preservation (i.e. self similarity of the velocity distribution and of the turbulent stresses) of a turbulent wall-jet may only be possible in especially tailored pressure gradient[19]. Nevertheless many investigators managed to collapse some of the data, the mean velocity profiles in particular, on self similar plots. Using a Gallilean transformation one should consider $(U_{max}-U_\infty)$ to be a dominant quantity governing the development of the flow. When local value of $[(U-U_\infty)/(U_{max}-U_\infty)]$ was expressed as a function $f(\eta)$ (where $\eta = Y/Y_{m/2}$ represents the dimensionless distance from the wall while $Y_{m/2}$ is the distance measured from the surface where the quantity $[(U-U_\infty)/(U_{max}-U_\infty)] = 1/2$) most of the mean velocity profiles measured in each data-set, collapsed onto a single curve (figure 8). The collapse was much better when $U_\infty/U_j \leq 0.4$ than for higher ratios of U_∞/U_j. The shape of the mean velocity profile was affected by the ratio U_∞/U_j while a change in Re_j did not result in a visible alteration of the normalized shape of the velocity distribution. The rate of spread of the wall jet is greatly affected by the velocity ratio and by Rej (fig.9). It varies almost linearly in the direction of streaming as it did in the absence of external flow.

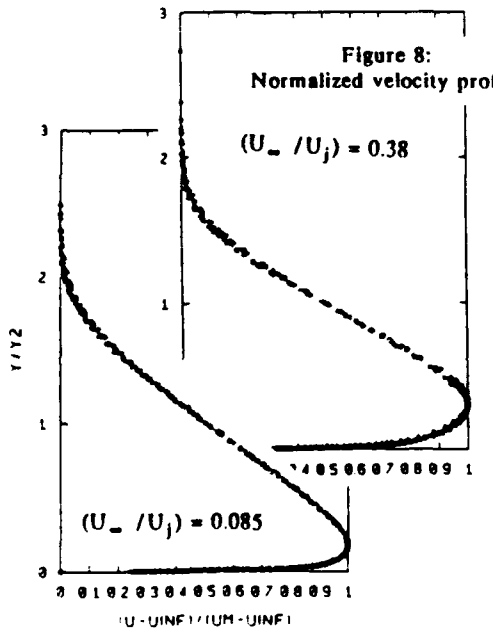

Figure 8:
Normalized velocity profiles

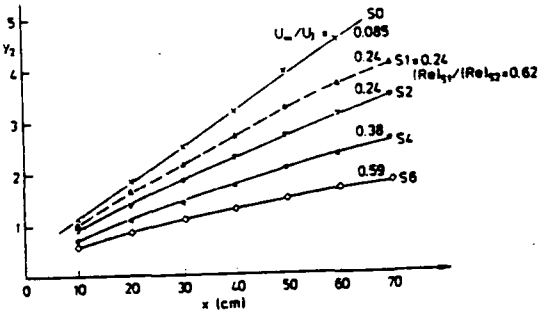

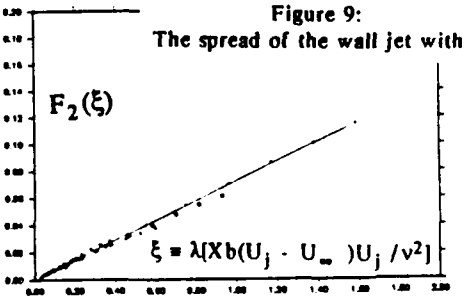

Figure 9:
The spread of the wall jet with X

The fully developed wall jet in the absence of an external stream attains a local equilibrium which is independent of the detailed conditions at the nozzle[18,20]. The sole parameter determining the evolution of the jet is it's initial, kinematic momentum flux, J. This approach scaled correctly the three most important parameters in the wall jet: the width of the flow $Y_{m/2}$; the decay of the maximum velocity in the jet, U_m and the local wall stress, τ_w.

$$\frac{U_m \nu}{J} = F_1(\xi) \quad ; \quad \frac{Y_{m/2} J}{\nu^2} = F_2(\xi) \quad ; \quad \tau_w/\rho \left[\frac{\nu}{J}\right]^2 = F_3(\xi) \qquad (3)$$

where:

$\xi=[XJ/\nu^2]$ while $J=[U_j^2\, b]$ and U_j is the jet velocity at the nozzle exit. The width of the slot is b; ρ and ν are the density and kinematic viscosity of the fluid respectively. X is a streamwise distance measured from the nozzle.

It made these parameters independent of Rej and enabled an independent evaluation of τ_w. The question of scaling took different proportions than originally anticipated because it appears that the flow was not scaled correctly in the past. The addition of a free stream complicates the problem because one regards the maximum velocity in the wall jet as an excess velocity over the

free stream, thus:

$$F_1(\xi) = [(U_m - U_\infty)\nu]/J \tag{4}$$

One has also to assume that the paramount parameter governing the flow is the excess momentum flux: $\int_0^\infty (u - U_\infty)udY$ which for a uniform jet velocity in the absence of an upstream boundary layer degenerates to $[b(U_j - U_\infty)U_j]$ leading to two possible definitions of the streamwise dimensionless distance ξ:

$$\xi \equiv [Xb(U_j - U_\infty)U_j/\nu^2] \text{ or } \quad \xi \equiv \lambda[Xb(U_j - U_\infty)U_j/\nu^2] \tag{5}$$

where: $\lambda \equiv (U_j - U_\infty)/(U_j + U_\infty)$

When the upstream boundary layer is thick, the simplified definition of excess momentum flux might no longer be adequate because one has to account for the momentum loss in the upstream boundary layer.

The utility of the definition of ξ becomes apparent when one substitutes the observed, self similar, normalized form of the velocity profile (figure 8), into the momentum integral equation which makes $\tau_w/\rho\,(\nu/J)^2$ a function of ξ, λ and on $[U_\infty/(U_m - U_\infty)]$ while being independent of Re_j. Therefore, when $[U_\infty/(U_m - U_\infty)]$ is assumed to be negligible, the similarity conditions of the wall jet in absence of an external stream are satisfied. When $(U_m \rightarrow U_\infty)$ a different set of conditions for self similarity prevail. This explains some additional difficulties in analyzing this flow.

THE FORCED TURBULENT WALL-JET WITHOUT AN EXTERNAL STREAM

This flow was examined first because of it is well known as being self similar with respect to the selected parameters. External excitation of free shear flows had a strong effect on a variety of time averaged quantities, like the mean velocity distribution, the rate of spread of the flow, the turbulent intensity and the Reynolds stress. It is thus natural to start the present discussion of the experimental results by exploring parametrically the effects of forcing on the same quantities in the wall jet.

A variety of forced flows were considered in the present experiment, they differed in jet momentum; slot width; frequency and amplitude of the imposed oscillations; and finally the manner in which forcing was introduced to the flow. A change in each one of the above parameters required concomitant traverses across the flow at various X locations. A sample of the data is shown in figure 10. The velocity profile plotted on the left (figure 10a) exhibits self similarity with respect to $Y_{m/2}$ and U_m irrespective of the X location while the profile plotted on the right (figure 10b) proves the existence of self similarity irrespective of the changes in all other parameters considered. Both profiles are compared to the dimensionless, unforced, velocity profile[18] and represented by a solid curves. One may conclude that two dimensional external excitation does not affect the normalized form of the velocity distribution within the range of parameters considered. Replotting the velocities adjacent to the wall on an expanded scale (figure 10c), and comparing them to unforced velocity measurements at otherwise identical conditions, indicate small but consistent differences between the two sets of data. These differences will be discussed later in some detail.

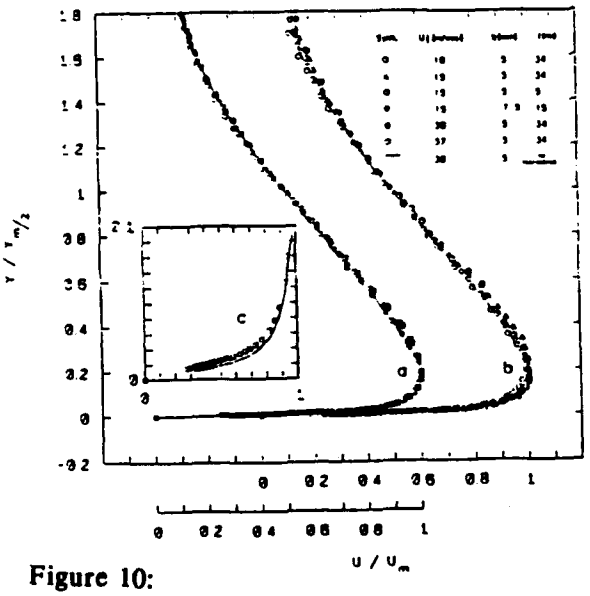

Figure 10:
Velocity profiles using self-similar coordinates:

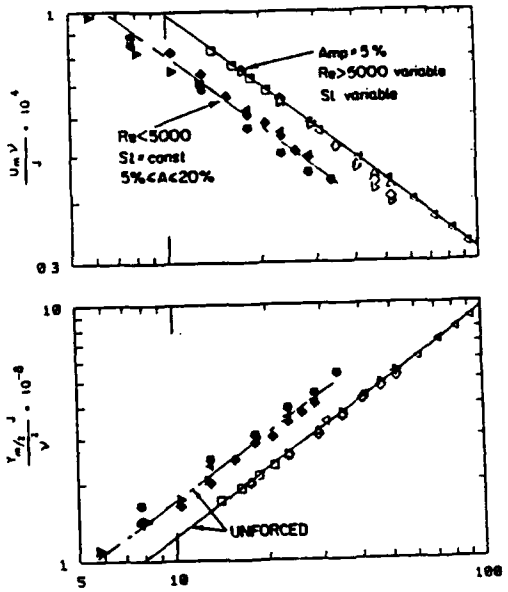

Figure 11:
The evolution of F_1 & F_2 with ξ

We were surprised to discover that neither the rate of spread nor the decay of the velocity scale were affected by the forcing. The solid lines drawn in figure 11 represent the unforced data accumulated for $Re_j \geq 7500$ while the broken lines correspond to $Re_j \leq 5000$. The symbols plotted represent data corresponding to various frequencies of excitation at nozzle Strouhal numbers ($St_j = f^*b/U_j$) varying between $3 \leq St_j{*}10^3 \leq 17$ (corresponding to $St = fv^3/J^2$ of $0.4 \leq St{*}10^{15} \leq 444$) and amplitudes, based on the streamwise velocity perturbation near the nozzle, ranging from 2% to 20%. Although some consistent differences depending on the level of forcing and on the Strouhal number can be detected they do not alter our initial conclusion about the lack of sensitivity of these mean-flow parameters to the external excitation. The cumulative effect of the threshold in Re_j occurring around $Re_j \equiv 5000$ appears to be much more significant then that of the two-dimensional excitation. Dimensional analysis of the independent parameters in the externally excited wall-jet suggests that variables other than ξ might affect the mean velocity distribution. Whenever the external excitation is harmonic, the broadening or the distortion of mean flow will depend on the square of the local amplitude of the velocity perturbations. In some cases the finite amplitude might be introduced directly by the forcing mechanism, while in others, the flow itself might act as an amplifier. We shall now examine the global effect of the excitation on the loss of momentum resulting from skin-friction drag. The velocities plotted in figures 10c suggest that forcing the wall jet might have an effect on the drag. Since the local skin friction was most conveniently determined from the slope of the mean velocity profile near the wall[18], the procedure was repeated presently in-spite of the fact that it is not considered in the literature as being very reliable[21]. The velocity measurements plotted in figure 12 are shown in dimensional form because this representation enables the reader to assess the quality and the amount of data acquired in the viscous sub-layer. Sometimes more than 10 data points were included in the linear fit made to the velocity profile near the wall. There is no doubt that even a relatively low level of forcing (the data plotted correspond to an initial amplitude of 2%) results in a reduction of the wall shear stress, τ_w. Heat loss from the hot-wire to the wall was assumed to be negligible[22] since the flow was turbulent and most of the data was taken at distances from the wall ranging from 50 to 80 wire diameters while the Re based on the wire diameter varied from 0.7 to 4.

Plotting $\tau_w/\rho\,(\nu/J)^2$ versus ξ and comparing the results with the skin friction measured in the absence of forcing indicates clearly the differences in τ_w in spite of the logarithmic scale chosen (figure 13). At no instance did τ_w increase above it's nominal unforced value. Reductions in the skin friction of approximately 10% were prevalent at most frequencies corresponding to initial excitation amplitudes which were lower or equal to 5%. However, reductions in τ_w of approximately 40% were also recorded by forcing at much higher amplitudes corresponding to

10% or 20% of the efflux velocity at the nozzle. Alternately, forcing at a preselected frequency which is amplified by the flow achieved the same drag reduction at a much lower input amplitude (figure 13).

In attempting to sort out the independent contribution of frequency; amplitude and Reynolds number on the local τ_w, one may assume that the dimensionless $\tau_w/\rho\ (\nu/J)^2$ depends on the distance from the nozzle (XJ/ν^2) and on the local amplitude of the coherent perturbations present in the flow regardless of their origin. We computed the phase-locked, ensemble-averaged velocity signals and from them deduced the local r.m.s. levels of the coherent motion. These quantities were then integrated across the flow to provide a measure of the intensity of the coherent motion at a given X station. It transpired that a local coherent motion having an average amplitude of 0.3% may be responsible for a reduction in τ_w of approximately 15% while an additional increase in local amplitude by a factor of 10 resulted in an incremental reduction in $\tau_w/\rho\ (\nu/J)^2$ of an additional 15% only. This suggests that the reduction in the local skin friction is not linearly dependent on the strength of the coherent motion.

A comparison was made between the mean velocity distributions of the forced and the unforced wall-jets in the vicinity of the surface by using the conventional "wall coordinates". It seems that external excitation modifies the velocity distribution in what appears to be the logarithmic region. It was shown that the slope, A, of the logarithmic profile ($U^+ = A \log Y^+ + B$) appears to be a universal constant and is equal to 5.5 while the additive constant B was strongly dependent on Re_j $(4 < B < 10)$. This conclusion applies to the forced wall-jet as well. It also appears that the logarithmic fit to the forced data may only be applied at larger values of Y^+ when compared to the unexcited flow.

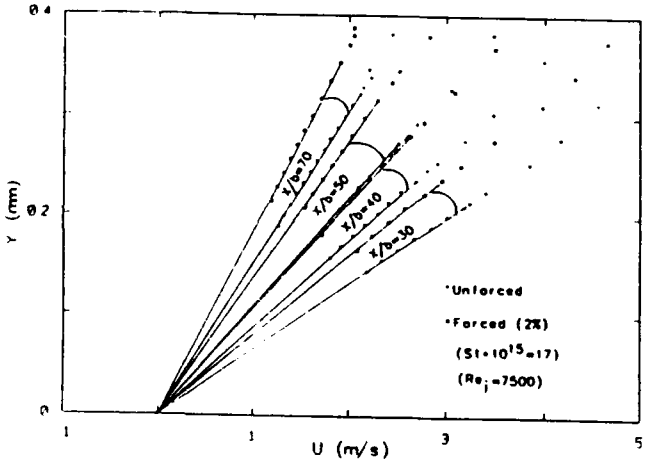

Figure 12:

The effect of forcing on dU/dY near the wall.

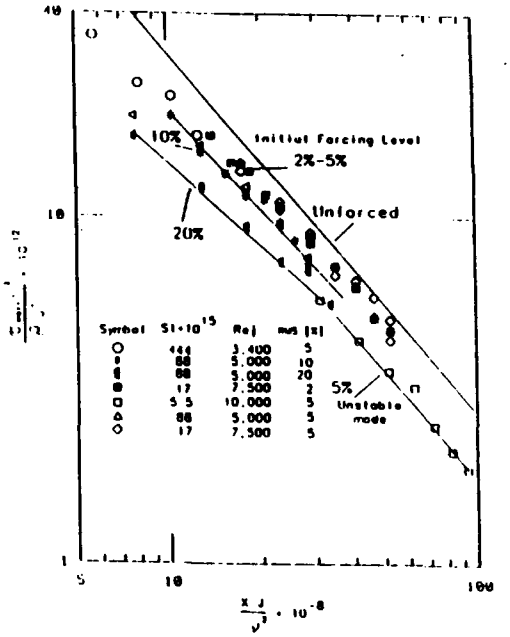

Figure 13:

The evolution of the dimensionless skin friction with ξ

Some of the underlying assumptions used in deriving the logarithmic velocity profile do not apply to the wall jet (i.e. that neither the logarithmic region is far removed from the location at which $Y=Y_m$ nor is the stress constant within that region). Consequently the existence of the logarithmic region appears to be somewhat fortuitous. The introduction of forcing did not only affect τ_w but also reduced the extent of the constant stress layer (fig. 14). The total and the viscous stress distributions in the inner part of the wall-jet are plotted at the top of this figure in order to assess the effects of excitation on these quantities. The wall-stress, which is entirely viscous at the surface, is reduced by the two dimensional forcing. However for $Y^+ > 10$, the effect of excitation on the viscous stress vanishes since forcing seizes to have an effect on the

mean velocity profiles in this region, and thus on $\nu(\partial U/\partial Y)$. At $Y^+ > 30$ where the contribution of the viscous stress to the total stress becomes vanishingly small, the latter decreases rapidly with increasing distance from the wall and changes sign between $60 < Y^+ < 100$ depending on the forcing and on Re.

The lateral distribution of turbulent energy production $[-(u'v')\partial U/\partial Y]$ with increasing distance from the surface, also plotted on figure 14, indicates that external excitation reduces the the Reynolds stress and with it the turbulent production. The integrated turbulent production in the inner region of the wall-jet between the surface and the location at which $Y = Y_m$ defined by:

$$\text{PRODUCTION} = \frac{1000}{(Um)^3}\int_0^{Ym} -(u'v')\,\frac{\partial U}{\partial Y}\,dY \qquad (6)$$

is reduced by an approximate factor of 3 when the flow was forced at St 10^{15} = 5.5 at X/b = 70 (i.e. forcing reduced the value of the production integral from 0.668 to 0.214). This is a significant effect which presumably alters the entire turbulent energy balance in this flow and not just the scales of the large coherent eddies. Since the mean velocity gradient vanishes at $Y^+ \equiv$ 150, the Y locations at which $u'v' = 0$ and at which $\partial U/\partial Y = 0$ do not coincide[23] leading to a region of a weak but negative turbulent production just below the location at which $Y=Y_m$.

Forcing the wall-jet reduces the turbulent intensity in the vicinity of the surface and this reduction is strongly affected by St while all other parameters are maintained constant. The reduction in u'/Uj exceeds in some places 25% as may be deduced from figure 15 (see arrow comparing one data point at X/b=40 and St=5.5 which provides an example). Since the production of turbulence increases the level of u', the reduction in u' due to forcing might be a direct result of the reduced production level near the wall.

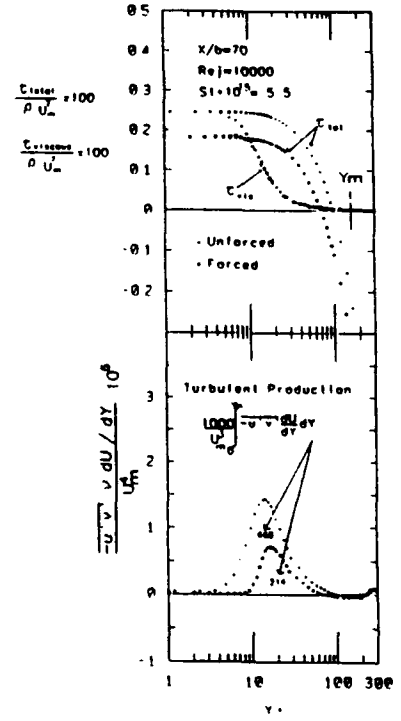

Figure 14:
The distribution of total and viscous stress and turbulent production near the surface.

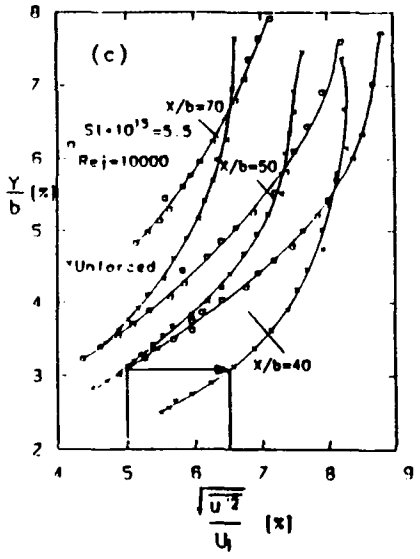

Figure 15:
The distribution of u' near the surface

THE EVOLUTION OF HARMONIC PERTURBATIONS IN THE WALL-JET AND WALL-WAKE

The propagation and amplification of small amplitude wavy disturbances, in slightly divergent free shear flows was discussed by Crighton and Gaster[24] and others. The application of this analysis to the wall jet is, in principle the same, with the exception of the "no slip" boundary conditions at the wall and the need to use the viscous form of the Orr-Sommerfeld equation.

This problem too was analyzed by Gaster[25] in conjunction with the stability of the divergent boundary layer. The stability of the non-divergent, laminar wall jet was considered by Tsuji et al[26]. We shall therefore, not repeat these derivations and only dwell on some specific aspects stemming from the application of this model to the turbulent wall jet.

Harmonic excitation of both flows enabled us to digitize the measured velocities at any streamwise location together with the forcing signal used to deflect the flap located at the apex of the wedge in the wall-wake case or near the nozzle in the wall jet. This signal, plotted at the bottom of each figure (in fig. 16) provided the necessary phase reference with respect to which other measurements taken anywhere in the flow could be referred and ensemble-averaged. Since there is a possibility of a subharmonic resonance the long time series were subdivided into segments which contain two waves of the forcing frequency. Samples of such phase-locked and ensemble averaged traces of the streamwise component of velocity are plotted above the forcing signal. The periodicity of the velocity signal is self evident but its harmonic distortion varies with Y. The least distorted signals appear at the outer edge of the flow where the velocity is not contaminated by turbulence.

One may observe a slow phase advance in the maximum velocity recorded in the wall jet with increasing distance from the wall provided $Y/Y_{m/2} < 1$. At this Y location, which approximately coincides with the inflection point of the mean velocity profile, a sudden phase shift occurs which is followed by a gradual phase delay with increasing Y. The data presented for the wall-wake accentuates the sudden phase shift in the outer flow. One may Fourier decompose these signals and plot the transverse distributions of amplitude and phase of the signals at the frequency of forcing. The transverse distribution thus obtained, is compared with the amplitude distributions calculated from the linear stability model. Both measured and calculated amplitude distributions are normalized by their local maxima which occurs fairly close to the wall.

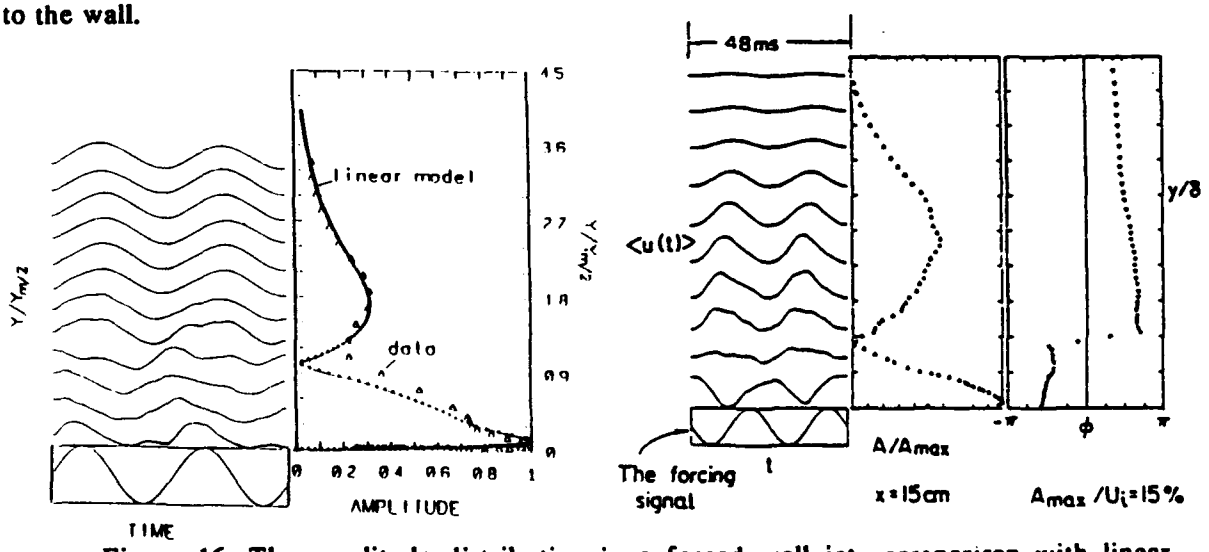

Figure 16: The amplitude distribution in a forced wall jet - comparison with linear model, & the amplitude and phase distribution in a wall-wake

When similar comparison was done in highly unstable, unbounded turbulent shear flows like the mixing layer, the interaction between the coherent motion and the incoherent turbulence was not accounted for. Since these flows were dominated by an inviscid instability the inviscid Orr-Somerfeld equation was solved, and the role of the Reynolds number did not have to be considered[5]. The primary instability in these flows is affected by viscosity in spite of the fact that they are also inviscidly unstable. The no-slip condition at the surface provides significant viscous stresses and enhances the dissipation which may cause the harmonic motion to decay. The incoherent turbulent fluctuations may increase this dissipation and the non linear interactions between the coherent and incoherent fluctuations may provide a cascade mechanism through which the effects of viscosity are enhanced. All these interactions, which are not accounted for in the model, might be lumped together into an equivalent viscous term by introducing an eddy viscosity[27-29]. Since the Reynolds number appears as a parameter in the Orr-Somerfeld equation a choice of a fictitious Re introduces an indeterminacy not present in the inviscid calculations. For example, the experimental results plotted in figure 16 agree reasonably well with theoretical

model provided the eddy viscosity was 10 times larger than the viscosity of the fluid.

The disturbances at the fundamental frequency in a wall-wake may also be viewed as an array of spanwise vortices extending across the entire boundary layer (fig.16). The 180° shift in phase which depicts the center of the eddies is convected along the surface at approximately one-half of the free stream velocity while moving away from the surface with increasing X.

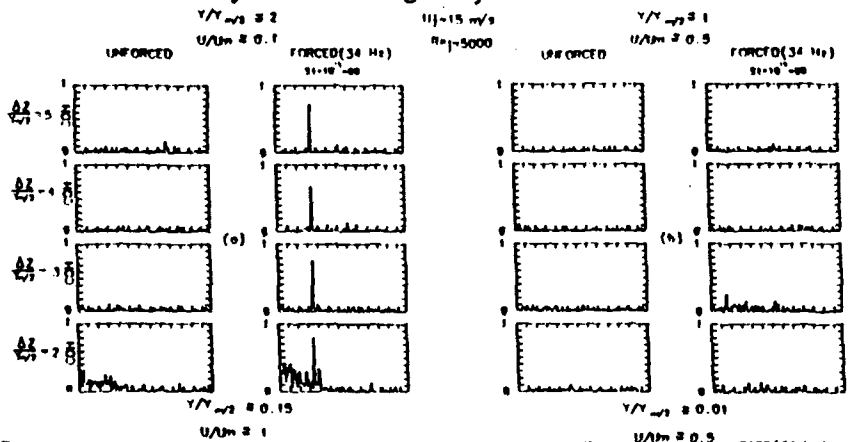

Figure 17: Spanwise coherence in a wall-jet

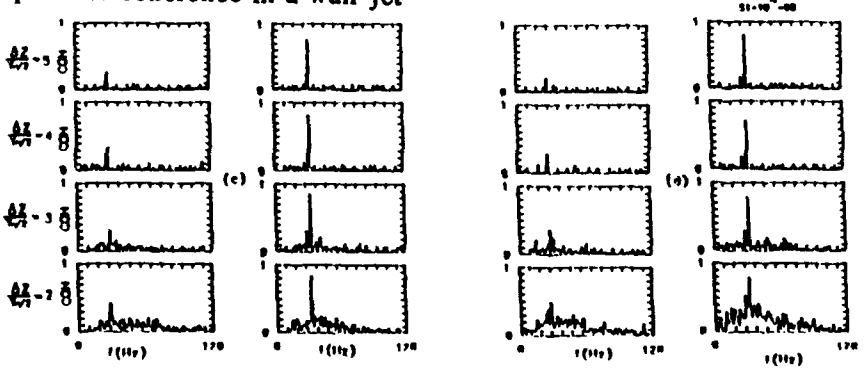

We shall now explore the changes that took place in the large scale structures in response to the external excitation. We shall particularly look for effects occurring near the solid surface in order to ascertain the reasons for the reduction in τ_w. The improvement in the two-dimensionality of the large scale structures is one such effect which had been observed in both the mixing layer and in the wake[4,30]. The coherence spectra of the velocity fluctuations, sensed by two probes separated in the spanwise direction provides a convenient measure of the degree of two dimensionality attributable to each scale (or frequency) of the motion. Two point correlations of the broad-frequency signal also yield a measure of two-dimensionality which is biased somewhat towards the most energetic eddies. The data plotted in figure 17 represents coherence at spanwise separation distances ranging from 10 to 130mm corresponding typically to more than 5 characteristic widths of the flow. The measurements were done at a variety of Y locations in the presence and in the absence of external excitation. The frequency chosen to be shown for the wall jet was 34 Hz corresponding to $St=fv^3/J^2=88*10^{-15}$. The results plotted in figure 17 correspond to four Y locations: starting at the outer edge of the wall-jet ($Y/Y_{m/2} \cong 2$), proceeding to the vicinity of the inflection point of the mean velocity profile ($Y/Y_{m/2} \cong 1$), going down to the location at which $U \cong U_m$ and ending in the vicinity of the wall. The spanwise coherence in the outer part of the unforced jet is negligible provided $\Delta Z/Y_{m/2} > 2$ (fig. 17a). For $\Delta Z/Y_{m/2} \leq 2$ the coherence in the unforced flow exceeds the value of 0.15 over a broad range of low frequencies and Y locations, suggesting that the large scale structures occurring naturally in the flow are somewhat coherent over this span. There is also a distinct peak in the coherence level around 30 Hz within the inner part of the unforced wall jet which is even noticeable at $\Delta Z/Y_{m/2} = 5$. If this St is associated with the natural coherence of the large eddies, then the forcing frequency used in the experiment is very close to being the frequency which undergoes naturally, the highest level of amplification at this particular X location.

External excitation increased the coherence to 0.75 at the outer edge of the wall-jet (fig.

17a) but failed to have any effect near $Y/Y_{m/2} = 1$ (fig. 17b). This effect may be explained with the aid of figure 16 which is representative of the coherent amplitude distribution of the streamwise velocity fluctuations in the forced wall-jet. The maximum amplitude of the coherent motion in the outer part of the jet occurs around $Y/Y_{m/2} = 1.8$ while the minimum occurs at $Y/Y_{m/2} = 1$ and therefore one should not expect any improvement in the coherence in the vicinity of this Y location. The improvement in the coherence observed in the inner region of the wall-jet (at $Y/Y_{m/2} = 0.15$ & 0.01) can also be associated with the relatively large amplitude of the local oscillations. It is interesting to note that the spanwise coherence in the forced wall-jet did not diminish by increasing ΔZ and it was actually higher near the surface than in the outer edge of the jet.

Similar measurements are also done in the wall wake (fig.18) where the maximum coherence in the unforced flow is approximately 0.3 beyond a separation distance of $\Delta Z = 30$mm which is commensurate with the local boundary layer thickness. External excitation increased this value to 0.8 over most of the boundary layer with the exception of the height above the wall where the local velocity $U/U_1 \equiv 0.7$. This height corresponds to the average location of the centers of the passing eddies as they were detected by the 180° phase shift in the phase locked amplitudes. Three dimensional plots of the spanwise correlation coefficient taken at various heights above the surface are shown in figure 19 for the forced and unforced flows. The contour plots representing the natural flow exhibit some periodic behavior near the surface of the wall jet but none near the surface of the wall wake because of the massive separation which occurs under these conditions. Forcing, not only increased the spanwise extent of the highly correlated region but made it much more periodic in time. The primary eddies appear to be two-dimensional and regular.

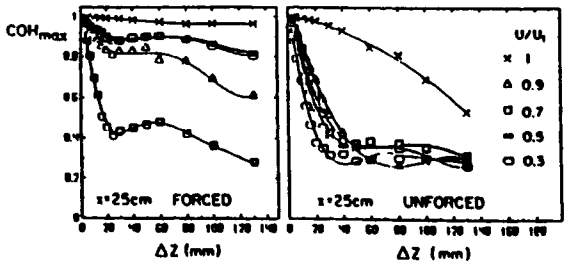

Figure 18: Maximum spanwise coherence in a wall-wake

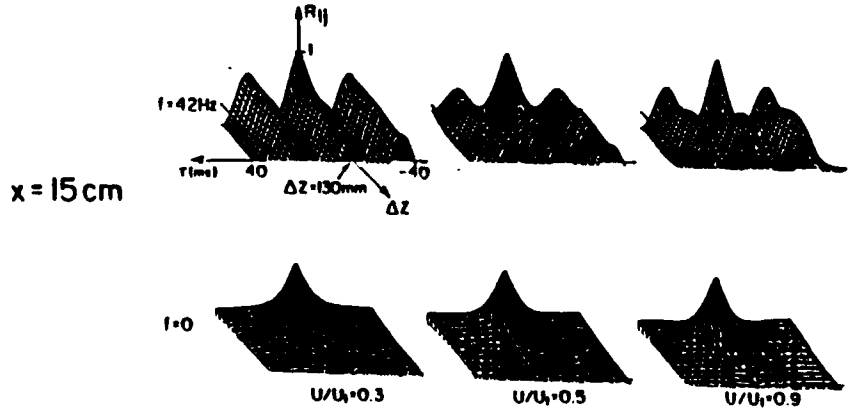

Figure 19: Correlation measurements in the T-Z plane of a wall-wake

The unexpected reduction in the mean-skin-friction prompted us to examine the phase locked distribution of this quantity over two periods of the forcing frequency. The data was based on the phase locked analysis of $[\partial\langle U\rangle/\partial Y]_w$ measured at various streamwise locations. The oscillations in the skin friction corresponded to the oscillations imposed on the flow. It is interesting to note that the maximum skin friction observed during any phase of the forced oscillation at any streamwise location was approximately equal to the mean skin friction of the unforced flow.

CONCLUSIONS

Two dimensional excitation of the wall-jet in the absence of an external stream has no appreciable effect on the rate of spread of the jet nor on the decay of it's maximum velocity. Careful examination of the flow near the surface (i.e. for $0 < Y^+ < 100$) reveals some profound differences which manifest themselves in reducing the skin friction. Local reductions of 30% in the wall stress, as a consequence of such an excitation, were not uncommon. The skin friction drag which is the only contributor to the loss of momentum in this flow was also reduced by a comparable amount. The production of turbulent energy near the surface was reduced resulting in lowering the intensities of the streamwise component of the velocity fluctuations. These effects, which were observed in the fully developed region of the wall-jet (i.e. at $X/b > 30$), are insensitive to the method of forcing but they are sensitive to the frequency and the amplitude of the excitation.

External excitation enhanced the two-dimensionality and the periodicity of the coherent motion. This enhancement is clearly visible near the surface and near the free interface of the turbulent flow. The large coherent structures in this flow might be identified with the most amplified, primary instability modes, of the mean velocity profile. Detailed stability analysis confirms this proposition though not at the same level of accuracy as it did in many free-shear flows.

The preliminary observations in the wall wake lead to similar conclusions and represent also a successful attempt to control and delay the separation of a turbulent boundary layer. The introduction of harmonic, two-dimensional oscillations results in a reattachment of the flow and changes the proportions between the "wake" and the "wall" functions whose linear combination represents the streamwise velocity distribution in a turbulent boundary layer. It does not, however, alter the universal form of these functions.

ACKNOWLEDGEMENT

The presentation was based on an M Sc. thesis of Mr. B. Nishri at Tel Aviv U. and on the work done in collaboration with Prof. M. Zhou, Dr. Y. Katz and Mr. E. Chorev at the University of Arizona. Both projects were supported in part by grants from AFOSR and monitored by Dr. J. McMichael.

REFERENCES

1 Willmarth, W. W., 1975a, *Annual Review Fluid Mech.*, 7:13.
2 Willmarth, W. W., 1975b, Structure of turbulence in boundary layers, in: "Advances in Applied Mechanics," Academic Press, New York.
3 Ho, C. M. and Huerre, P., 1984, *Ann. Rev. Fluid Mech.*, 16:365.
4 Wygnanski, I.., Champagne, F. and Marasli, B., 1986, *J. Fluid Mech.*, 168, p.31
5 Weisbrot, I. and Wygnanski, I., 1988, *J. Fluid Mech.*, 195, p.137-159
6 Hussain, A.K.M.F., 1983, *Physics of Fluids*, 26 2816-2850
7 Kline, S. J., Reynolds, W. C., Schraub, F. A., and Runstadler, P. W., 1967, *J. Fluid Mech.*, 50:133.
8 Falco, R.E., 1977, *Phys. of fluids Suppl.* 20,124
9 Hussain, A.K.M.F. and Reynolds, W.C., 1970, *J. Fluid Mech.*, 41, 241
10 Hussain, A.K.M.F. and Reynolds, W.C., 1972, *J. Fluid Mech.*, 54, 241-261
11 Craik, Alex, D.D., Wave Interactions and Fluid Flows, 1985, *Cambridge University Press*
12 Landhal, M.T., 1990, *J. Fluid Mech.*, 212, 593-614
13 Katz, Y., Nishri, B., and Wygnanski, I., 1989, AIAA Paper 89-0975.
14 Stratford, B.S.,1959, *J. Fluid Mech.*, 5, p.1-35.
15 Brown, G. L. and Roshko, A. 1974, *J. Fluid Mech.*, Vol 64, p. 775.
16 Bradshaw, P. 1967, *J. Fluid Mech.*, Vol. 29, p. 625.
17 Patrick, W. P. 1986, *United Technologies Res. Center Report* R85-915555.
18 Wygnanski, I., Katz, Y. and Horev, E., 1990, *J. Fluid Mech.*,
19 Irwin, H.P.A.H., 1973, *J. Fluid Mech.*, 61:33
20 Narasimha, R., Narayan, K. Y., and Parthasarathy, S. P., 1973, *Aeronautical J.*, 77:335.

21 Launder, B. E. and Rodi, W., 1981, *Prog. Aerospace Sci.*, 19:81.
22 Wills, J. A. B., 1962, *J. Fluid Mech.*, 12:3.
23 Kruka, V. and Eskinazi, S., 1964, *J. Fluid Mech.*, 20:555.
24 Crighton, D.G. and Gaster, M., 1976, *J. Fluid Mech.*, 77, p.397
25 Gaster, M., 1974, *J. Fluid Mech.*, 66, p.465.
26 Tsuji, Y., Morikawa, Y., Nagatani, T. and Sakou, M., 1977, *Aeronautical Quarterly*, Vol XXVIII p.235
27 Tam, C.K.W. and Chen, K.C., 1979, *J. Fluid Mech.*, 92, p.303
28 Liu, J.T.C., 1971, *Phys. Fluids*, 14,, p.2251.
29 Marasli, B. Champagne, F.H. and Wygnanski, I.J., 1989, *J. Fluid Mech.*, 198, p.255-273
30 Wygnanski, I., Fiedler, H., Oster, D. and Dziomba, B., 1979, *J. Fluid Mech.*, 93, p.325